

MSc Thesis

Evaluation of an Ammonia Fueled Combine-cycle Gas Turbine Power System on Maritime Usage

Zheng Zhou
2021



EVALUATION OF AN AMMONIA FUELED COMBINE CYCLE GAS
TURBINE POWER SYSTEM ON MARITIME USAGE

A thesis submitted to the Delft University of Technology in partial fulfillment
of the requirements for the degree of

Master of Science in Marine Technology

by

Zheng Zhou

August 2021

An electronic version of this thesis is available at <http://repository.tudelft.nl/>.

Zheng Zhou: *Evaluation of an ammonia fueled combine cycle gas turbine power system on maritime usage* (2021)

© This work is licensed under a Creative Commons Attribution 4.0 International License. To view a copy of this license, visit <http://creativecommons.org/licenses/by/4.0/>.

The work in this thesis was made in the:

Department of Maritime and Transport Technology
Faculty of Mechanical, Maritime and Materials Engineering
Delft University of Technology

Student number : 4870786

Project duration: October 2020 – August 2021

Thesis committee: Ir. K. Visser, Rear-Admiral (ME) ret., Chairman of committee
Dr.Ir. L. van Biert, Supervisor
Prof.Dr.Ir. S. Klein, External member

ABSTRACT

Ammonia fuel has been widely considered as an attractive solution for reducing the green house gas emissions over recent years. Adapting ammonia as fuel on ships would highly reduce the carbon footprint of international shipping and off-shore transportation. Among the different systems currently under development for carbon-free power production in the near future, the combined-cycle gas turbine system stands out for its relatively high system efficiency and a potential for running on pure ammonia fuel while maintaining a low level of NO_x emission. This thesis project puts a sight on a special design of this type of COGAS power system and tries to adapt it for maritime usage onboard future ships.

Previous researches have pointed out the key design features of the ammonia COGAS power system being running under a high fuel-air ratio with a cooling method based on EGR technology and cracking the additional ammonia fuel into hydrogen in the gas turbine system, then this created hydrogen concentration could be used for re-heating the exhaust before it is used by the combined steam cycle. However, current understanding of this type of COGAS system is still limited under static analysis and designed working points. This thesis project tries to provide a basic view on the off-design performance and dynamic behaviors of this COGAS system, and examines if this system is still able to maintain a low level NO_x emission under such working conditions.

This thesis project combines a dynamic model of an ammonia gas turbine and a chemical thermodynamic model for simulating the chemical behavior of the work fluid inside the gas turbine system. It is found that the fuel-air equivalence ratio of the gas turbine needs to be designed at a high value to ensure the flammability of the hydrogen consisting exhaust in the re-heating process. A very low NO_x emission is observed in the gas turbine exhaust under an assumption of complete chemical reactions. The final NO_x emission of the COGAS system is found to be within the EEDI Tier III limitation under both rated and part-load working conditions. The thermal efficiency of the gas turbine is relatively low due to the high equivalence ratio, while a system efficiency comparable with current oil-fueled COGAS power system is able to be expected for the full system of ammonia COGAS.

On the phase of dynamic analysis, this project has concluded that traditional fuel control method for controlling gas turbine power generation is not adaptable to gas turbine systems working at fuel-rich conditions. A non-linear behavior is observed due to this high equivalence ratio. This thesis provides a new controlling method with controlling both the fuel injection ratio and the EGR ratio with an additional feedback controlling system attached to the original feed-forward system of the fuel control. Basic tests shows that such method is able to generate a dynamic output with the correct tendency. This thesis project also observes a high sensitivity of NO_x emission with the presence of additional oxygen in the exhaust under a complete chemical reaction.

In this thesis project it is found that the considered ammonia COGAS system maintains the advantage of traditional COGAS power systems and is able to take an advantage in comparing with medium-speed diesel systems under an ammonia economy. Power output of the ammonia gas turbine is able to be controlled with a combination of fuel control and EGR control. A low NO_x emission within the limit of EEDI Tier III is observed under both rated and part-loading conditions of

the power system, but this is achieved with the assumption of a complete chemical reaction. Whether this assumption is adaptable to maritime scaled ammonia gas turbine system requires further kinetic analysis on the combustion process and further research efforts in the designing of the combustor system.

ACKNOWLEDGEMENTS

This report is written to conclude my study at the Delft University of Technology for the degree of Master of Science in Marine Engineering.

Great efforts have been made in finishing this project during the past months. At this stage I would like to express my gratitude to Dr. Ir. Lindert van Biert, who have been my daily supervisor though out this project, and leads me to a new level of understanding on dynamic modelling and how to carry out this research project.

I would also like thank Ir. Klaas Vissor, chief supervisor of this project, who have provided valuable guidance on scheduling the scope of this project and gave professional advises on the tasks from a maritime point of view.

Besides, there is a special thank to Dr. Ir. Peter de Vos and the local branch of IMarEST in TU Delft, who have inspired me on this project from the very beginning.

Lastly, as this project has suffered a great interruption due to the COVID-19 pandemic, hereby I would like to thank for my parents, my fellows and friends and everyone else that help me through these hard days, and together towards the better future of this world.

Zheng Zhou
August 2021

...

CONTENTS

1	INTRODUCTION	1
1.1	Background	1
1.2	Ammonia as Alternative	1
1.3	The gas turbine solution	2
1.4	Conclusions from literature review	4
1.4.1	Feasibility of COGAS in maritime	4
1.4.2	Ammonia combustion in gas turbines	7
1.4.3	Summary	11
1.5	Research objectives and scopes	12
1.5.1	Research objectives	12
1.5.2	Project scope	12
1.6	Thesis outline and unique contribution	13
2	MODELLING OF THE TURBINE SYSTEM	15
2.1	The general ideas	15
2.1.1	Characteristics of gas turbines	15
2.1.2	Scaling parameters	20
2.2	Dynamic characteristics	21
2.3	Chemical solver	23
2.4	System layout	25
2.4.1	EGR block	25
2.4.2	Compressor	25
2.4.3	Combustor	26
2.4.4	Driving Turbine	26
2.4.5	Power turbine, shaft and additional components	28
2.5	Chapter summary	29
3	STATIC MODEL VERIFICATION	31
3.1	Verification of the chemical model	31
3.2	Verification of compressor and turbine maps	32
3.3	Verification over complete system	33
3.4	Chapter summary	34
4	STATIC PERFORMANCE OF THE AMMONIA GAS TURBINE	35
4.1	Design point of the gas turbine	35
4.1.1	Defining fuel injection	35
4.1.2	System performance at designed point	36
4.2	Overview on off-design performance	38
4.2.1	Turbine inlet temperature	38
4.2.2	Pressure ratios	39
4.2.3	Power and efficiencies	40
4.3	Discussion on emissions	41
4.4	Summary	43
5	DYNAMIC BEHAVIOR AND CONSIDERATIONS OVER CONTROLLING PROCESS	45
5.1	Fuel control method and application	45
5.2	Discussing the result	48
5.3	A new controlling solution	49
5.3.1	Checking of the idea	50
5.3.2	Discussing on the new method	51
5.4	Other observations	53
5.5	Summary	54
6	CONCLUSIONS AND RECOMMENDATIONS	55
6.1	Answers to the research questions	55
6.2	Additional conclusions and recommendations	57

A	MATLAB CODE FOR CHEMICAL MODEL	64
B	GENERAL VIEW OF THE SIMULINK MODEL	72
C	STATIC RESULTS	74

LIST OF FIGURES

Figure 1.1	Volumetric and gravimetric energy density of logistic fuels including the tank system	2
Figure 1.2	T-S diagram of Brayton cycle	3
Figure 1.3	T-S diagram of ideal combined-cycle power system	5
Figure 1.4	Experiment results and simulations of laminar flame speed in ammonia oxidization	8
Figure 1.5	Respective plots of ignition delay time for ammonia and methane	8
Figure 1.6	Adiabatic flame temperature with fractions of several products at distribution of Equivalence ratio.	9
Figure 1.7	Variations of mole fractions in flame structures with a variety of equivalence ratios	9
Figure 1.8	Equilibrium NO concentration at the boiler outlet as a function of equivalence ratio at PR=20 for different EGR ratios . .	10
Figure 1.9	TIT as a function of equivalence ratio at PR=20 for different EGR ratios	11
Figure 2.1	Cross section of GE LM2500	16
Figure 2.2	Compressor and turbine performance map of an MGT	19
Figure 2.3	Compressor map approach block of the Simulink model.	20
Figure 2.4	Compressor map of GE LM2500	21
Figure 2.5	Layout of compressor block	25
Figure 2.6	Layout of chemical model block	26
Figure 2.7	Layout of combustor block	26
Figure 2.8	Layout of high-pressure turbine block	27
Figure 2.9	Outside look of high-pressure turbine block	27
Figure 2.10	Outside look of condensing block	29
Figure 2.11	re-heater	29
Figure 3.1	Comparison of calculated TIT with previous research	32
Figure 4.1	H ₂ concentration and TIT with different fuel injections.	36
Figure 4.2	TIT T ₂ of the gas turbine over different fuel injection ratios .	39
Figure 4.3	H ₂ concentration and TIT with different fuel injections	39
Figure 4.4	Power output of the gas turbine against fuel injection ratios. .	40
Figure 4.5	System efficiency of the gas turbine against fuel injection ratios.	41
Figure 4.6	NO _x emission against exhaust temperature of the gas turbine.	42
Figure 5.1	Fuel-flow rate characteristic	46
Figure 5.2	Dynamic output of the mass flow with fuel injection ratio reduced from 80% to 60%.	47
Figure 5.3	Dynamic output of shaft speed with fuel injection ratio reduced from 80% to 60%.	47
Figure 5.4	Dynamic output of the TIT with fuel injection ratio reduced from 80% to 60%	48
Figure 5.5	Dynamic output of the mass flow with the provided controlling process.	50
Figure 5.6	Dynamic output of the compressor outlet pressure with the provided controlling process.	51
Figure 5.7	Dynamic output of the mass flow with the provided controlling process.	51
Figure 5.8	Dynamic output of the mass flow with the provided controlling process.	52
Figure 5.9	O ₂ concentration output at gas turbine exhaust.	53
Figure 5.10	NO _x concentration output at gas turbine exhaust.	54

LIST OF TABLES

Table 3.1	Verification results of the compressor block.	32
Table 3.2	Verification results of the high-pressure turbine block.	33
Table 3.3	Verification results of the power turbine block.	33
Table 3.4	Comparison of numerical calculation and model outputs at designed point.	34
Table 4.1	H ₂ concentration and TIT with different fuel injections	36
Table 4.2	Data output for the designed point of the ammonia gas tur- bine model.	37
Table 4.3	Data output for different fuel injections of the ammonia gas turbine model.	38
Table 4.4	Output data against different fuel injections.	42
Table 5.1	Static data of the selected working conditions.	46

ACRONYMS

GHG	green house gases	1
SSAS	Solid State Ammonia Synthesis	1
ICE	internal combustion engine	2
SFC	specific fuel consumption	3
MGT	micro-gas turbine	3
SOFC	solid oxidizer fuel cell	3
COGAS	combined gas turbine and steam	4
SOFC-GT	solid oxidizer fuel cell - gas turbine	4
HRSG	heat recovery steam generator	4
EGR	exhaust gas recycling	10
EEDI	Energy Efficiency Design Index	10
TIT	turbine inlet temperature	10
PR	pressure ratio	10
TR	temperature ratio	16
ODEs	ordinary differential equations	13
DAEs	differential-algebraic system of equations	22

NOMENCLATURE

Latin symbols

T, t	temperature
c	heat capacity
H	enthalpy
S	entropy
p	pressure
\dot{m}, f	mass flow
Q	heat
P	power
n	polytropic index
N	shaft speed
J	rotational inertia
G	torque
	Gibbs free energy
U	internal energy

Greek symbols

π	pressure ratio
τ	temperature ratio
γ	heat capacity ratio
η	efficiency
ω	rotational speed

Vectors

α	efficiency vector
t	function vector
y	function vector
C	constant vector
A till H	NIST vectors

Subscripts

0	initial condition
1	compressor inlet
2	compressor outlet
	combustor inlet
3	combustor outlet
	turbine inlet
g	driving turbine outlet
	power turbine inlet
4	power turbine outlet
c	compressor
cb	combustor
t	turbine
pt	power turbine
b	adiabatic
s	isentropic
p	pressure
B	break power
td	turbine power system
sys	system
in	input
out	outlet
tot	total
$steam$	steam cycle
air	fresh air
che	chemical reaction
TIT	turbine inlet temperature

1

INTRODUCTION

1.1 BACKGROUND

Over the recent decades, the shipping industry has been highly influenced by the targets of limiting pollution. The International Maritime Organization (IMO) has adopted variant measurements to reduce green house gases (GHG) pollution, with ambition to reduce the CO₂ emissions of each tonnage-mile of cargo shipping by no less than 40% by 2030, and total annual GHG emissions by at least 50% by 2050[1]. The later goal has made it insufficient to cover the gap by switching to LNG fuel[2]. Biomass is also considered insufficient as the production takes over large amount of land and the price of such energy sources has not been able to be reduced over the years[3]. These factors has made it possible for other carbon-free chemicals to compete with or even taking advantages against the carbon-based chemicals in being used as alternative fuel sources. Among these alternatives, ammonia (NH₃), which as a carbon-free chemical has been considered to have the potential to be an attractive choice[4].

1.2 AMMONIA AS ALTERNATIVE

For a century, ammonia has been being a major chemical product and been transported overseas, mainly used in the agricultural fertilizer industry and cooling systems. Historically ammonia is produced with the Harber-Bosch process (Reaction 1),



which is able to to store energy efficiently[5]. Recent developments have also provided possibilities to generate ammonia more efficiently and more directly from renewable sources, which is called Solid State Ammonia Synthesis (SSAS) and is shown as Reaction 2[6].



As a nitrogen-based alternative fuel, ammonia contains no carbon or sulfur components and would be free from considerations of SO_x and Carbon based GHG pollutants. Besides, unlike LNG and hydrogen, ammonia does not require a very low temperature which is lower than -162°C to be liquefied, and is able to be stored at either a slightly low temperature of -33°C or under pressure[4] This makes it an adaptable energy carrier on board maritime structures.

Yet despite being mass produced and easy to store, there are also drawbacks for applying ammonia as a maritime fuel source. First of all, the volumetric energy density of ammonia is much lower than that of HFO with considering the tank systems, as shown in Figure 1.1. This means when applying ammonia as fuel it requires 3.3 times of room on the ship comparing with fossil bunkers. Moreover, the corrosive nature of ammonia due to its high acidity constant makes the storing tanks require special treatments, and sensors should be introduced to detect the

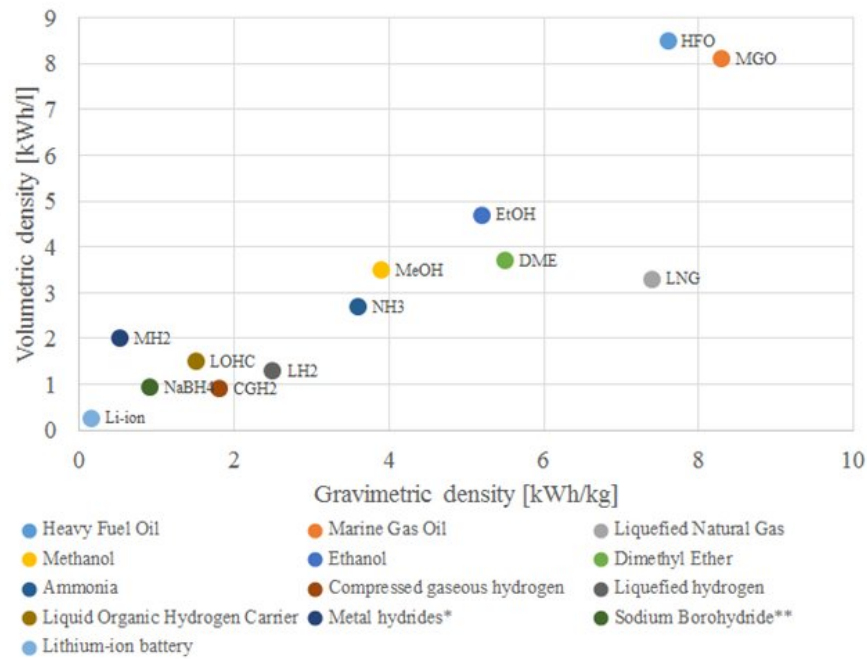


Figure 1.1: Volumetric and gravimetric energy density of logistic fuels including the tank system.[8] * Low temperature AB₂, Ovonic, ** Fuel 30, wet spent fuel

corrosion from an early stage and prevent a system failure[7].

Apart from the previous problems, what might be the most serious concerns on ammonia fuel are the hardness in ignition and NO_x emission in the exhaust. Ammonia has a very high ignition point of 652°C much higher than that of hydrogen (520°C) and MDO (250°C)[9][10]. From safety perspective this is a positive fact, while such a high ignition point combining a high ignition delay time makes the ignition process of ammonia combustion hard to carry out[11]. On the other hand, from practical results the NO_x emission of an ammonia burning internal combustion engine (ICE) is going to be much more significant and harder to reduce comparing with that of MDO. From works done by Reiter et.al.[12] the NO_x emission can go as high as 1000 ppmv with a 5%-95% diesel-ammonia mixture. Tests from Ryu et.al.[13] provides an even worse case, which the NO_x emission goes up to 5000ppm at break power.

Considering such drawbacks, it might have been a suggestive idea to try finding alternative power systems that has a potential to operate on ammonia while keeping a low emission level. This leads to the thought of whether a gas turbine system is able to handle such task to run on ammonia fuel while keeping a low rate of emission, since gas turbine operates with a continuous flame which avoids reversal ignition processes and has been maintaining a relatively low NO_x emission comparing with ICEs while running on common fossil fuels.

1.3 THE GAS TURBINE SOLUTION

Over the years, gas Turbines have been well known of their high specific power output at a cost of relatively lower thermal efficiency. Different from the ICEs, a gas turbine follows the Brayton cycle, and burns its fuel continuously at a high pressure. Instead of finishing the entire cycle within the combustion volume, the high temperature, high pressure combustion exhaust is later used to drive a single or multiple turbines to generate power output while also supplying power to drive the compressor, which on the other hand provides the high pressure fresh air for the

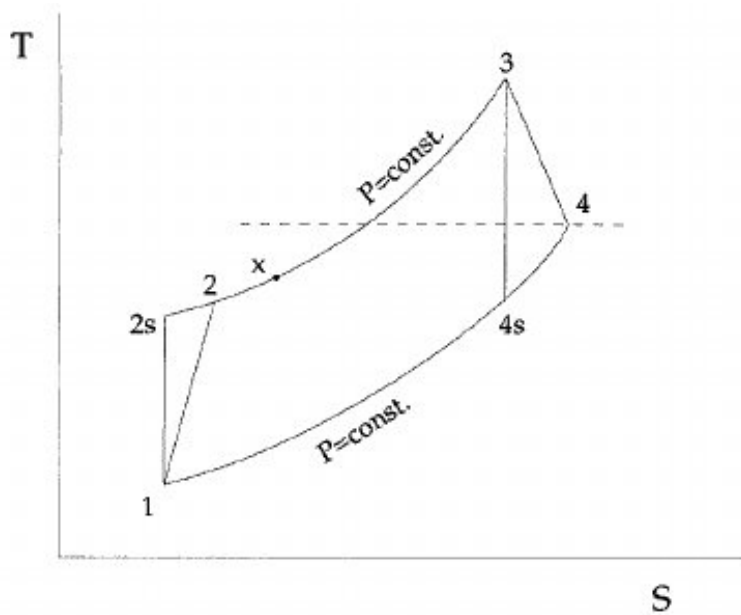


Figure 1.2: T-S diagram of Brayton cycle, with the ideal loop of 1-2s-3-4s-1, and the thermodynamic loop of 1-2-3-4-1[14]

combustor. The ideal and thermodynamic Brayton cycles are shown in Figure 1.2. For ammonia combustion, there is a major advantage for gas turbines that the continuous combustion process does not require frequent ignitions, which is quite different from ICES. With higher rotational speeds of the engine, the time for an ICE to finish its combustion cycle decreases sharply. Since ammonia has a high ignition temperature and a longer time delay in its combustion process[11], this may lead to problems in high speed engines. For ICES, one method to partly avoid this problem is to inject hydrogen as a helper in the combustion process, of which the hydrogen can be created from ammonia via a solid oxidizer fuel cell (SOFC) system[15]. However, with avoiding this frequent ignition process, a gas turbine may have the possibility to run on pure ammonia fuel, and hence reduce this additional system complexity as well as the related costs.

In previous time, it was considered not feasible to have gas turbines running on pure ammonia. However, most recent studies have demonstrated stable generation of power from pure ammonia combustion in a micro-gas turbine (MGT) with a high combustion efficiency and relatively low NO_x emission. Okafor et.al.[16] have developed an efficient design of gas turbine combustor which is able to run on pure ammonia and reach a combustion efficiency of 99.5% while controlling the NO_x emission within the level of 42ppmv. Kinetic modelling research have also provided possibilities to develop an effective combustor that runs on pure ammonia fuel[11]. Hence it is safe to say that a gas turbine power system that runs on pure ammonia fuel is feasible.

On the other hand, even though it is considered achievable to construct a GT system running on ammonia, the low efficiency of gas turbine systems still blocks its widely usage. Comparing the specific fuel consumption (SFC), the GE LM2500, which is a typical gas turbine for maritime usage, has an SFC of 227 g/kWh, while on the other hand an MAN V32/44 middle speed maritime diesel has an SFC of 173 g/kWh[17][18]. This is mainly due to that the exhaust temperature of a gas turbine is much higher than that of a maritime diesel, which is again due to its mechanical characteristics. Introducing more complicated processes such as recuperation can help reduce the SFC ratio, yet it highly increases the system complexity, weight, cost

and is only adaptable when the exhaust temperature is higher than the compressed inlet air. Moreover, adapting such processes is still not enough to cover the gap completely. Due to this high fuel costs, within the maritime world gas turbine systems are mostly used on super yachts, fast ferries and naval vessels which requires a high speed while the fuel cost is able to be trade-off with other performances. Further attempting of gas turbine application are commonly considered non-practical.

However, despite the failing in the maritime world, gas turbine systems have achieved great success in on-shore power plants. Heavy gas turbine products from Siemens, GE and other manufacturers have achieved system efficiencies of over 60%, much higher than any type of middle or high speed diesel engines[17]. This high system efficiency is achieved by applying a combined cycle, in which the exhaust gas after gas turbine expansion is used to heat up steam for another steam turbine. With the combined cycle, heat within the relatively high temperature GT exhaust is able to be reused and generated into power output. Practices of the combined gas turbine and steam (COGAS) maritime power system with original fossil fuels has shown a possible system efficiency of over 50%[19]. This gives the possibility of mounting an ammonia driven gas turbine onto merchant ships with a combined cycle power system, since the limitation of requiring MDO instead of cheaper HFO as the fuel for gas turbine systems does not exist anymore under an ammonia economy.

1.4 CONCLUSIONS FROM LITERATURE REVIEW

Even though the COGAS solution seems to be a good alternative for operation with ammonia based alternative fuel, the current understanding of such a power system is yet insufficient for locating the research gap before applying such power systems in maritime usage. A further digging-in on the characteristics of such power system is required and is carried out in the literature study of this project.

In the literature study, different solutions of ammonia power systems are analyzed and evaluated in order to prove the feasibility of the COGAS system being the potential choice for maritime usage under the ammonia economy. Following that, analysis on the combustion process of ammonia fuel is also made for a deeper investigation on the project. The Conclusions of this literature review is provided in the following sections.

1.4.1 Feasibility of COGAS in maritime

Although it has been suggested that a COGAS turbine system could be an attractive solution for the ammonia economy, there are yet multiple choices for the future ship power system that runs on ammonia. In order to prove the feasibility, an evaluation is made in the literature study to compare the COGAS system against a solid oxidizer fuel cell - gas turbine (SOFC-GT) combined system and the current middle speed diesel system. As described by its name, the COGAS system combines a gas turbine as the main power generator and a heat recovery steam generator (HRSG) system. Figure 1.3 shows an ideal COGAS combined cycle in T-S diagram, which combines a a simple Brayton cycle and a Rankine cycle. From this diagram, it can be found that with a relatively low working temperature, the steam cycle is able to cover much of the thermal losses of the gas turbine which has a high exhaust temperature, hence increases the system efficiency. Typical COGAS systems for the state of art mostly have a system efficiency around the value of 52%[21]. Yet on the other hand, the additional HRSG system increases the complexity and cost of the system.

middle speed diesel systems in the near future[24]. For the SOFC-GT hybrid system, on the other hand, the advantages on efficiency becomes even more recognizable. The advantage against the middle speed diesels can be higher than 20 percent[22].

The power density of the COGAS system is higher than that of both the low and medium speed ICEs as well as maintaining a better flexibility for arrangement, while the SOFC based solution would require much more weight and volume than a middle speed diesel system.

From analysis provided by F. Haglind[25], half of the engine room is emptied when replacing the diesel propulsion system by a COGAS system on a pro-panamax container ship. Other studies also shows an additional 2.5% of cabins could be placed if the medium speed diesels are replaced by COGAS on a cruise ship[26]. On the contrary, currently the gravimetric power density of typical SOFC systems are around the range of 100-140W/kg, while the value for a typical MAN medium speed ICE is able to reach around 1000W/kg[18][27][28].

Results over system cost

Even though the installation cost of both power systems are higher than the diesel solution, the COGAS power system is managed to compete against the diesels with the help of good port facilities under the green ammonia economy. Yet the SOFC-GT hybrid solution may have to further lower its system price before is able to be considered worth of considering.

For the COGAS system, a typical combined-cycle system of a GE LM2500 gas turbine may cost around \$22.5 to \$26.5 million USD, with the cost of a single LM2500 gas turbine being around \$8 to \$9 million USD[21]. This results in the cost shifts around the range of \$550/kW to \$800/kW depending on the system lay-out. The cost of SOFC systems are even more significant, with the estimated manufacturing cost of the near future still being over \$1000/kW and a market price even higher[29].

In previous years, the COGAS system is considered much more costly on operation than that of a middle speed ICE system[30]. However, this is mainly due to that the price of marine diesel oil (MDO) is much higher than that of heavy fuel oil (HFO)[27], which is a situation that does not exist anymore under the ammonia economy. In the previously mentioned analysis, it is suggested that a cruise ship with a 58MW COGAS power system would have an estimated fuel consumption of 46120t of fossil fuel annually, comparing with the number of a similar scale middle speed diesel system being 46590t[30]. Yet in this comparison, COGAS system is considered of suffering heavy costs due to part load working condition when the ship is in port without an access of shore power, which is considered as 3120 hours annually with a 15MW power being completely wasted[30]. With better shore power supplies being available over the years this could be considered a kind of unfair. With eliminating this part of load, it would result in an additional 2819t of fuel saving and is able to make a significant advantage for the COGAS power system. Considering an estimation that the price of green ammonia bunker basing on energy equivalent becomes as low as the price of current MGO, which is estimated as \$500 per metric ton basing on historical bunker price in Rotterdam[27], the total fuel saving of 3289t fuel of MDO equivalent would result in an \$1.64M of annual cost reduction.

Results over technical readiness

The state-of-art of this technology provides a high possibility for the COGAS system to be available in the near future, while it would require much more effort to make a fuel cell based power system available by the coming decade.

Nowadays there have already been COGAS systems installed on commercial ships[25]. Hence the research goal is to adapt this power system to the ammonia fuel. Currently it has been proven that pure ammonia is able to be combusted in a MGT[16]. However the detailed design of such combustor components are yet to be adapted to real scale gas turbine systems. Besides, current understanding on the thermodynamic behaviors of ammonia fuel combustion is yet within static level[31], hence the performance under dynamic workloads is also required to be investigated.

On the other hand, fuel cell systems have been struggling with system cost, power density and system scaling over the past decades. Several prototype products have been provided by Siemens and Mitsubishi for system testing[32][33]. Yet up to now fuel cell systems are usually provided within the size of hundred kilowatts[29][32][33]. Hence it is hard to state that the SOFC-GT hybrid system is able to cover the power requirement of large scale commercial ships, which would typically require an output of several megawatts.

With the results of the basic evaluation, the commercial readiness of the SOFC-GT system is considered too low to meet the requirements of limiting green house gas emissions in the next decades, and the COGAS power system is selected to be the preferable solution of becoming an alternative of the middle speed diesel systems, which has difficulties in running on pure ammonia fuel and have to implement additional treatments. In order to make the ammonia COGAS power system available for commercial usage in the shipping business, however, further analysis is required to look into the thermal chemical performance of pure ammonia combustion in the gas turbine combustor.

1.4.2 Ammonia combustion in gas turbines

In order to have a further understanding on the current stages of thermodynamic research on ammonia combustion, analysis over both chemical kinetic research and a more simplified lumped-parameter thermodynamic model are provided by the literature research. An up-to-date CFD model is introduced and be used for explaining the thermal chemical behaviors of ammonia fuel during its combustion process. After that, the thermodynamic model from Keller et.al.[31] and its performances are further analyzed for its adaptation of representing the chemical processes which take parts in the thermodynamics of a gas turbine combustor. The conclusions are displaced as follows.

On chemical kinetics

The ignition delay time of pure ammonia fuel is much longer than that of more sensitive carbon-based fuels.

Basing on previous works done by Metcalfe et.al.[34] and Song et.al.[35], Otomo et al.[11] have improved the kinetic model and simulations of laminar flame speed matches the experiment results over different equivalence ratio more accurately than previous models. Song et al.[35] provides the oxidization path of ammonia at high pressure under oxidizing conditions, shown in Reaction 3,



Otomo et al.[11] further improves the elementary processes relevant to NH_2 , HNO and N_2H_2 intermediates, and shows that these intermediate chemicals play a key role in improving the reaction mechanisms of ammonia oxidization. The results of different simulations on laminar flame speed is shown in Figure 1.4.

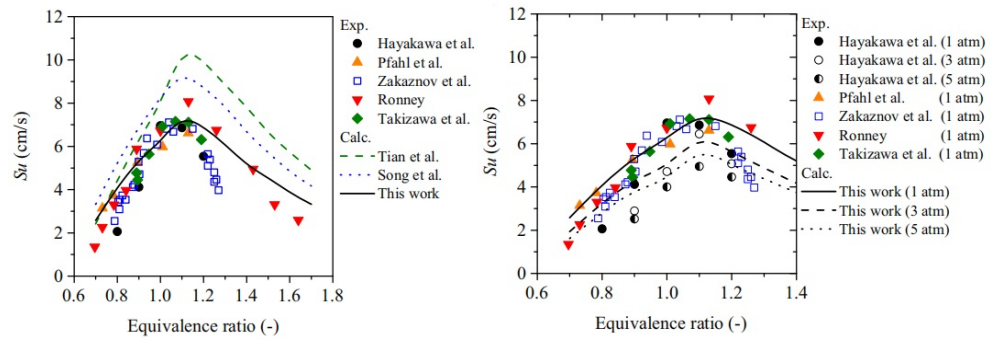


Figure 1.4: Experiment results and simulations of laminar flame speed in ammonia oxidation[11]

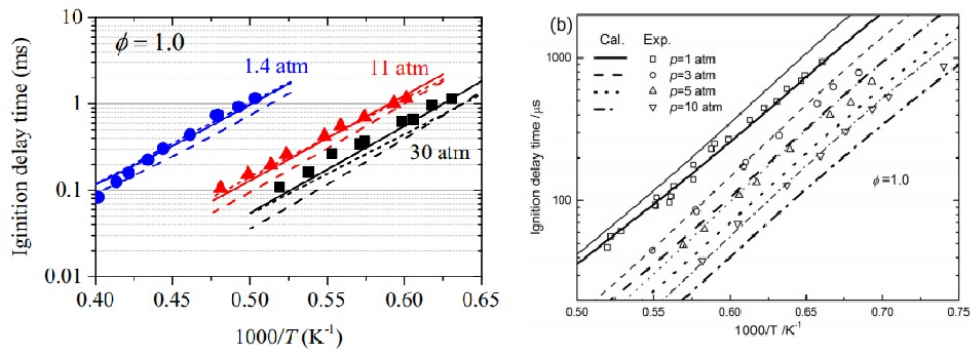


Figure 1.5: Respective plots of ignition delay time for ammonia and methane[11][36]

With the improved kinetic model, Otomo et al.[11] further analysis the ignition delay time of ammonia, and gets comparable results with multiple experiments. Figure 1.5 shows the ignition time delay of ammonia and methane respectively, from which a significant difference can be observed.

Ammonia has a slightly lower adiabatic flame temperature than carbon-based synthetics.

With the kinetic calculation from Otomo et al.[11], the adiabatic flame temperature of ammonia combustion is estimated to be 2050K with an equivalence ratio of 1. This result is comparable with data from other resources, which varies from 2023K to 2123K[9][37]. This is a relatively low value comparing with carbon-based synthetics such as methane, which has an adiabatic flame temperature of over 2200K[9]. This lower flame temperature has brought difficulties to the combustion process, yet it also decreases the difficulty in designing the cooling methods for matching the material limits of the turbo-inlet temperature in a gas turbine.

A fuel-rich condition, hence an fuel-air equivalence ratio higher than 1.0 is more appreciated for ammonia combustion, in which process the additional ammonia is reformed into nitrogen and hydrogen.

With the equivalence ratio increase from 1 to 1.25, the fraction of NO drops sharply while uncombusted ammonia begins to increase at an equivalence ratio of 1.1 due to incomplete combustion. In the meantime, hydrogen is generated from cracking ammonia during the combustion process. The concentration of hydrogen in the reaction product increases steadily with the gaining of equivalence ratio until reaching a mole fraction of 5×10^2 at the equivalence ratio of 1.1 and remains around that value. This is shown in Figure 1.6.

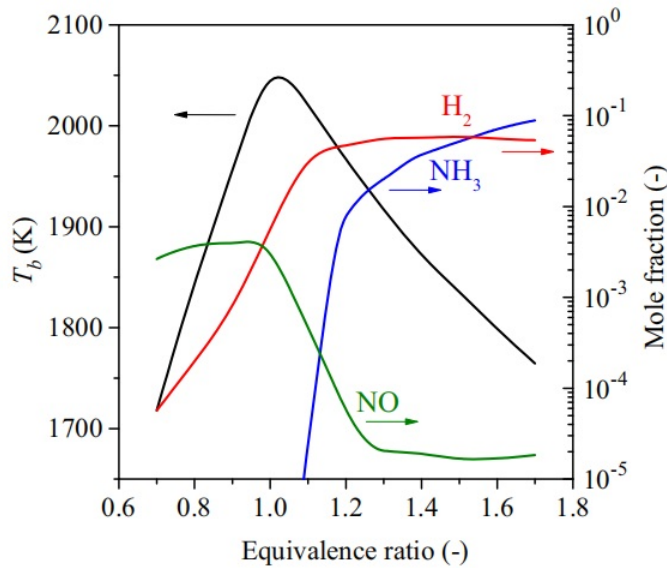


Figure 1.6: Adiabatic flame temperature with fractions of several products at distribution of Equivalence ratio.[11]

Additionally, the kinetic model provides the variations of mole fraction of the chemicals in a structure of the flame length, which is displayed in Figure Figure 1.7 for the equivalence ratio of 0.7, 1.1, 1.3, and 1.5 respectively. From these plots it is possible to conclude that for these variant equivalence ratios, the chemical reaction process is able to be finished within the flame structures between 1.5cm to 2cm. This indicates that the combustion process is completed fast enough within the scale of the combustion chamber, hence allows a more simplified thermodynamic model to be introduced as representing the combustion process for analyzing the concentration of different products.

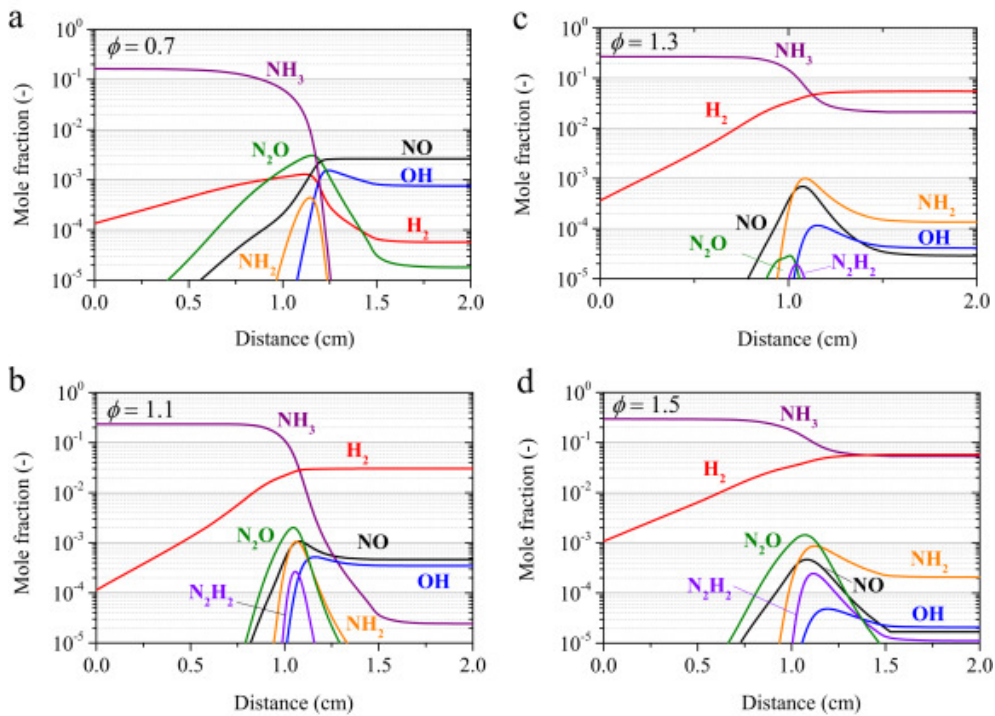


Figure 1.7: Variations of mole fractions in flame structures with a variety of equivalence ratios (0.7, 1.1, 1.3, and 1.5) in NH_3/air at 1 atm[11]

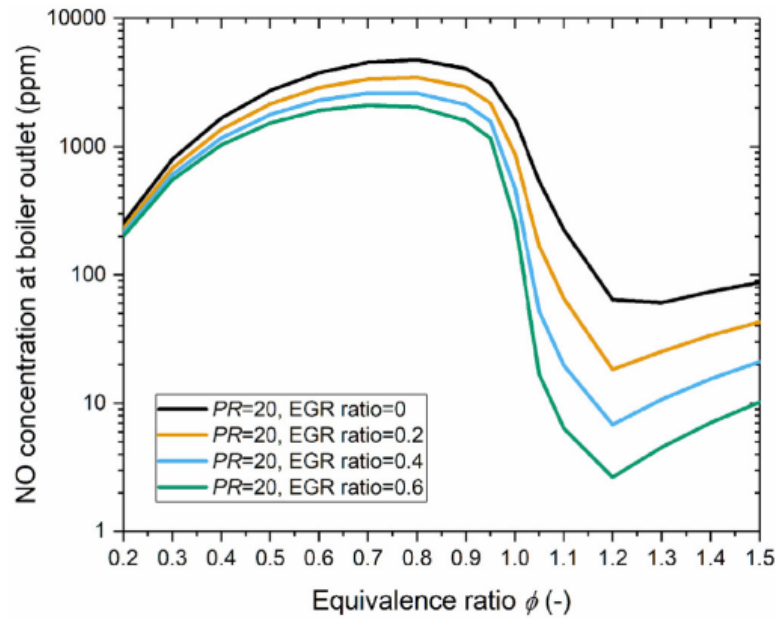


Figure 1.8: Equilibrium NO concentration at the boiler outlet as a function of equivalence ratio at PR=20 for different EGR ratios[31]

On Lumped-parameters analysis

Under fuel-rich conditions, especially for the equivalence ratio being higher than 1.1, the NO_x formation drops dramatically.

With the thermodynamic calculations, Keller predicts the NO_x concentration in the exhaust of ammonia fueled gas turbines with a pressure ratio (PR) of 20 and 5 respectively[31]. The NO_x emission is represented by the concentration of NO because the formation of N₂O and NO₂ are orders of magnitude smaller than that of NO. The NO concentration of the gas turbine exhaust is shown in Figure 1.8 with the pressure ratio of 20 and different exhaust gas recycling (EGR) ratios, and is distributed to the equivalence ratio. With the equivalence ratio being higher than 1.1, the NO formation drops dramatically to the range of around 100ppm, comparing with that being over 1000ppm for lower equivalence ratios and is able to match the Energy Efficiency Design Index (EEDI) Tier III requirement[38].

Exhaust gas recycling is required to control the turbine inlet temperature (TIT) of the ammonia gas turbine.

It has been evaluated by earlier studies that using the EGR process is a good choice for a combined cycle gas turbine running under fuel-rich conditions[11]. Due to emission concerns, the injected cooling gas of an ammonia gas turbine is required to be oxygen free. This prevents the application of introducing additional fresh air. From Keller's evaluation, with an EGR ratio of 0.6 it is able to keep the turbine inlet temperature under 2000K at all the considered equivalence ratios[31]. The distribution of calculated turbine inlet temperatures over equivalence ratio and different EGR ratios are shown in Figure 1.9.

High system efficiency is able to be reached with the ammonia COGAS system, yet there are still remaining questions regarding on the system distribution.

With a fuel-rich condition of around 1.2 equivalence and a high EGR ratio of 0.6, the considered power system with conservative estimations of the compressor and turbine efficiencies (0.85 and 0.8 respectively) is able to reach a system efficiency

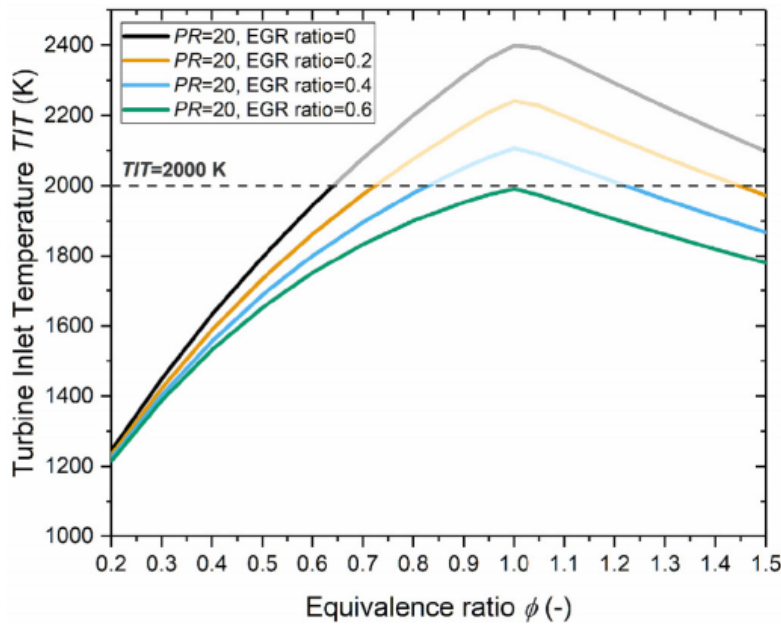


Figure 1.9: TIT as a function of equivalence ratio at PR=20 for different EGR ratios[31]

around 56%[31]. Considering that hydrogen is generated during the fuel-rich combustion, which has been mentioned in Section 1.4.2, it is suggested to combust this hydrogen product for reheating the exhaust before using it to generate steam for the heat-recovery steam cycle[31]. However, whether the hydrogen concentration is high enough to be ignited still needs further analysis.

Despite these achievements, the evaluation of the thermodynamic behavior is yet provided under steady state and a designed operation conditions. This further leads to the need of studying on the chemical behavior with a dynamic model of the gas turbine system, which is able to predict the results under part load or switching conditions.

1.4.3 Summary

In the literature study, different solutions of combined cycle gas turbine power system are analyzed and evaluated for an adaptation of becoming the potential choices for maritime usage while operating on ammonia fuel. Basing on the results of the evaluation which shows the COGAS solution could be the better choice under the ammonia economy in the near future, further analysis is made for a deeper investigation on the combustion process of ammonia fuel. Chemical kinetic results revealed a preference in the fuel-rich condition for ammonia oxidization in order to limit the NO_x pollutants. A further thermodynamic evaluation shows the feasibility of a COGAS power generation system running on pure ammonia fuel under the fuel-rich condition with the assistance of EGR technology.

With these achievements, the current research gap is located for the target of adapting the ammonia COGAS power solution on a ship. Different from the on shore power plants, the power system on a ship may operate under off-design conditions and switching more frequently. However, with the former researches being provided under static state operations, there is yet a lack of further digging in on the behavior of such an ammonia fueled gas turbine system over a dynamic changing load. This gap has lead to the task of building a dynamic model of the ammonia gas turbine for analyzing the chemical thermodynamics under such working conditions.

1.5 RESEARCH OBJECTIVES AND SCOPES

1.5.1 Research objectives

The literature study has revealed the feasibility for adapting an ammonia-fueled COGAS system as the power system for a ship in the near future. Previous researches also suggest that such a gas turbine system should operate under fuel rich conditions in order to limit NO_x pollution. With the help of EGR technology, such an ammonia gas turbine system is proven to be feasible, but the evaluation process is yet limited to a static analysis. Considering that the working principles of maritime power systems are much different from on-shore power plants, the main research question is listed as following:

What is the thermal-chemical performance of an ammonia gas turbine system under dynamic operation.

To answer the main question, the following sub questions need to be answered:

Sub question 1: To what level will the emissions be changed under off design conditions?

In previous researches, emissions are not well evaluated for the off-design conditions of such an ammonia gas turbine system. Hence to what level will the concentration of the pollutants be shifted under the off design conditions and during the shifting process is worth considering.

Sub question 2: To what level can the system be controlled to try minimizing the pollutants?

Controlling of the power systems are always important regarding on system performance and limitation of emissions. This should also be adaptable to the ammonia gas turbine. Hence to what level can this be improved?

Sub question 3: How much reduction in NO_x pollution can be achieved compared to the current ICE systems?

Even though the ammonia gas turbine may still require a scrubber system for dealing with the pollutants, how much saving can be achieved is yet an interesting research question to look into. This reduction may also turn into significant competitiveness for the ammonia gas turbine system.

Sub question 4: How can a dynamic model be constructed for an ammonia gas turbine system?

From previous analysis, it is suggested that a lumped parameters ODE model will be built for the simulation process. However, the determination of the modelling details are yet to be made and these details may highly influence the final results. The modelling process needs to be provided with utterly carefulness. Correct verification and adaptable validation processes are also required to guarantee the correctness and validity of the dynamic model.

1.5.2 Project scope

Basing on the conclusions from the literature review, the feasibility of adapting the chemical thermodynamic methods are proven by the kinetic evaluations. Hence a dynamic lumped parameters model of the ammonia gas turbine focusing on the

combination of chemical thermodynamics of the combustion process and the gas turbine dynamics is able to be applied for this project. The governing equations of the dynamic properties will be provided in ordinary differential equations (ODEs) in order to simplify the testing process of the model. Chemical thermodynamic is included for prediction of the reaction products. These performances are going to be calculated by minimizing the Gibbs free energy of the considered control volumes. Besides the chemical component and the dynamic conservation laws in each component, the model should also be able to represent the typical off design behaviors of a common gas turbine system. A basic control system may also be required for the model to represent its switching process.

While on the other hand, considering the fact that the COGAS system have already been tested on current ships, the HRSG system of the combined cycle will not be considered in this project. Detailed controlling systems and the power distributions are also excluded from the scope due to the limitation of current materials available. With conclusions of the literature review, chemical kinetics are considered not to be covered in the scope since the chemical processes are able to be considered finished within the scales of each of the control volumes. Losses other than what has taken into account in the thermodynamic efficiency are also not considered, since the thermodynamic efficiency of the gas turbine has been considered representative enough for analyzing the dynamic properties of such a system[39].

1.6 THESIS OUTLINE AND UNIQUE CONTRIBUTION

This thesis is based on the thermodynamic evaluation provided by Keller et al.[31] by combining the same method of chemical equilibrium calculation with a dynamic model of gas turbine system. This extends the analysis into part load performances and its controlling method over power switching situations, hence further adapts the ammonia COGAS power system with maritime requirements. In the following chapters, the construction and combination of the model is going to be presented with the research questions be answered step by step.

In Chapter 2, the structure of the combined model is going to be displayed and discussed. In Chapter 3, the static results at the designed point of this combined model is going to be compared with previous researches in order to have the model verified. Following that, static results of the model over different design and off design points are going to be analyzed in Chapter 4, concentrating on system performance and NO_x emissions. Chapter 5 will be focused on the dynamic processes and evaluate the difference in the controlling method of the gas turbine under high equivalence ratios.

2

MODELLING OF THE TURBINE SYSTEM

To solve the research questions, a model has to be built consisting both the mechanical and chemical components. From the mechanical phase it needs to represent the dynamic behaviors of a typical gas turbine, from the chemical phase should represent the chemical reactions being considered in different stages of the COGAS system. In this chapter the layout of this model is going to be discussed, including the basic characteristics of the two phases and the association between different components. Firstly, an overview of the gas turbine characteristics is provided in Section 2.1, giving a basic understanding of the gas turbine system to be simulated. Following that, what is required in different components of the model to represent the dynamic behaviors will be shown in Section 2.2. With the mechanical requirements being satisfied, the representative of the chemical process is carried out in Section 2.3. Then with all the materials being gathered, the general layout of the model is provided in Section 2.4. After this model being constructed, further checking and testings are able to be done before the model is used to solve the research questions.

2.1 THE GENERAL IDEAS

By definition, a model is a simplified representation of a system in time or space intended to promote understanding of the real system[40]. In order to fulfill the requirement of building a dynamic model of the ammonia gas turbine, a basic understanding of the gas turbine system has to be provided. Basing on the characteristics of a real system, different estimations can be introduced to simplify the model system.

2.1.1 Characteristics of gas turbines

A simple cycle gas turbine that follows the basic Brayton cycle contains four main components, the compressor, the combustor, the turbine and the power turbine. Figure 2.1 shows a cross section of a typical maritime gas turbine. The inlet air is first compressed in the compressor. Then fuel is injected under the high pressure and combusted in the combustor. After that, the high pressure, high temperature exhaust gas drives the turbine, which supplies the required power to the compressor via a driving shaft. The power output is generated via the power turbine driven by the exhaust gas. For some heavy duty gas turbines, this could be simplified into a single shaft design, in which the turbine and the power turbine is combined and drives a single shaft to supply mechanical power to both the compressor and the load. However this is not adaptable for maritime gas turbines, since the load of the turbine is time varying and an alternative shaft provides more freedom for matching the speed and power output of the power turbine.

In order to reduce the system complexity while maintaining the main characteristics of a maritime gas turbine, the gas turbine system is going to be built as a two shaft system. There is a single set of compressor which is driven by the high pressure turbine via the first shaft, and the load is delivered by the low pressure power turbine through the second shaft. The two shaft design keeps the compressor

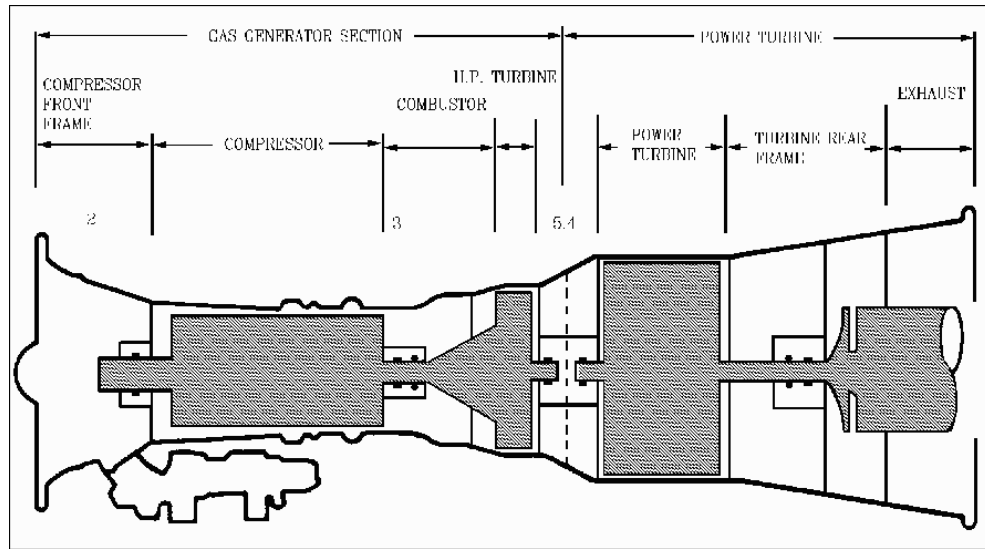


Figure 2.1: Cross section of GE LM2500[41]

and high pressure turbine being able to work under the best matched speed with changing loads while the power turbine is able to be kept at a stable speed, which is mandatory when driving a generator on modern ships.

Real gas turbine systems are frequently compared with the ideal Brayton cycle for evaluating the system. As an ideal model, the ideal Brayton cycle applies several assumptions[39]:

- Compression and Expansion processes are considered isentropic.
- The change of kinetic energy of the working fluid is accounted by using total temperature and overall pressure.
- No pressure losses are considered.
- The working fluid has the same composition and is a perfect gas with constant specific heats.
- Heat is added to the working fluid from an external source instead of what is in the actual process.
- Heat is extracted from the working fluid with a heat sink instead of what is in the actual process.
- Constant mass flow throughout the cycle, hence fuel flow being neglected.

With these assumptions, the characteristics of the ideal Brayton cycle can be calculated. Under this condition, the PR across the compressor is the same as that of the turbine, shown as Equation 2.1.

$$\pi_c = \frac{p_2}{p_1} = \frac{p_3}{p_4} = \pi_t \quad (2.1)$$

Besides, the temperature ratio (TR) of the gas turbine is defined as Equation 2.2.

$$\tau = \frac{T_3}{T_1} \quad (2.2)$$

Traditionally, the outlet temperature is calculated by adapting the Poisson's p-T relation:

$$\tau_c = \frac{T_2}{T_1} = \left(\frac{p_2}{p_1}\right)^{\frac{\gamma-1}{\gamma}} = \pi^{\frac{\gamma-1}{\gamma}} \quad (2.3)$$

$$\tau_t = \frac{T_3}{T_4} = \left(\frac{p_3}{p_4}\right)^{\frac{\gamma-1}{\gamma}} = \pi^{\frac{\gamma-1}{\gamma}} \quad (2.4)$$

Hence the formulas are distributed like the follows:

$$T_2 = T_1 \left(\frac{p_2}{p_1} \right)^{\frac{\gamma-1}{\gamma}} = T_1 \pi^{\frac{\gamma-1}{\gamma}} \quad (2.5)$$

$$T_4 = T_3 \left(\frac{p_4}{p_3} \right)^{\frac{\gamma-1}{\gamma}} = T_3 \left(\frac{1}{\pi} \right)^{\frac{\gamma-1}{\gamma}} \quad (2.6)$$

However, instead of applying this transformation directly, the GPSA Engineering Databook has been processing a new way in calculating the isentropic outlet temperature of the compressor and turbine stages since its 13th edition[42]. The formula is shown as Equation 2.7 and 2.8, with η_c and η_t being the isentropic efficiency of the compressor and the turbine respectively.

$$T_2 = T_1 \left[\frac{1}{\eta_c} \left(\pi_c^{\frac{\gamma-1}{\gamma}} - 1 \right) + 1 \right] \quad (2.7)$$

$$T_4 = T_3 \left\{ \eta_t \left[\left(\frac{1}{\pi_t} \right)^{\frac{\gamma-1}{\gamma}} - 1 \right] + 1 \right\} \quad (2.8)$$

Since it has been stated that the GPSA equations have a better performance comparing with Equation 2.5 and 2.6, these equations are going to be adapted in estimating the temperature difference in the compressor and turbine stages in this project.

With the temperature difference being defined, the compressor and turbine power can be concluded as follows:

$$P_c = \dot{m}(H_2 - H_1) \quad (2.9)$$

$$P_t = \dot{m}(H_3 - H_4) \quad (2.10)$$

The output power of the ideal turbine is distributed as Equation 2.11:

$$P_B = P_t - P_c \quad (2.11)$$

With the definition of the system efficiency being divided by the total heat input of fuel injection, the thermodynamic efficiency of the ideal gas turbine is shown as Equation 2.12:

$$\eta_{td} = \frac{P_B}{Q_{in}} = 1 - \left(\frac{1}{\pi} \right)^{\frac{\gamma-1}{\gamma}} \quad (2.12)$$

The calculations above are adapted for a single stage turbine system. Yet for this project the driving turbine and the power turbine are separated. For an ideal two shaft turbine system the power of the driving turbine needs to match with that of the compressor. This leads to the following equations for calculating the power delivered by the two turbines:

$$P_t = P_c = \dot{m}(H_3 - H_g) \quad (2.13)$$

$$P_{pt} = P_B = \dot{m}(H_g - H_4) \quad (2.14)$$

With adapting the ideal assumptions:

$$P_t = P_c = \dot{m}c_p(T_3 - T_g) = \dot{m}c_p T_1 \tau \left[1 - \left(\frac{1}{\pi_t} \right)^{\frac{\gamma-1}{\gamma}} \right] \quad (2.15)$$

$$P_{pt} = P_B = \dot{m}c_p(T_g - T_4) = \dot{m}c_p T_1 \left(\pi_{pt}^{\frac{\gamma-1}{\gamma}} - 1 \right) \quad (2.16)$$

Where π_t and π_{pt} refers to the pressure ratios of the turbine and the power turbine respectively. Notice that there is the following internal relationship between these pressure ratios no matter the ideal assumptions being adapted or not:

$$\pi_{tot} = \pi_t \cdot \pi_{pt} \quad (2.17)$$

The equations above has provided the method for calculating the performance of an ideal gas turbine system. However, in a real gas turbine there are multiple losses that needs to be considered. Usually the losses in the compressor and the turbine, which by far are the most significant, are taken into account when estimating the thermodynamic properties of a gas turbine[39]. This makes the processes of compression and expansion no longer isentropic, hence the isentropic index kappa needs to be replaced by a polytropic index n, with the relationships:

$$\frac{\gamma - 1}{\gamma} = \frac{1}{\eta_c} \cdot \frac{n_c - 1}{n_c} \quad (2.18)$$

$$\frac{\gamma - 1}{\gamma} = \eta_t \cdot \frac{n_t - 1}{n_t} \quad (2.19)$$

Where n_c and n_t being the polytropic index of the compressor and the turbine respectively, and the η_c and η_t being the efficiency of the compressor and the turbine respectively.

Considering these thermodynamic losses, previous formulas for calculating isentropic temperature differences of the compressor and the turbine should be modified as Equation 2.20 and Equation 2.21 respectively[42].

$$T_2 = T_1 \left[\frac{1}{\eta_c} \left(\pi_c^{\frac{n_c-1}{n_c}} - 1 \right) + 1 \right] \quad (2.20)$$

$$T_4 = T_3 \left\{ \eta_t \left[\left(\frac{1}{\pi_t} \right)^{\frac{n_t-1}{n_t}} - 1 \right] + 1 \right\} \quad (2.21)$$

Basing on these equations, the static performance at the designed point of the gas turbine system is able to be estimated. But in a gas turbine system there are also correlations among the mass flow, the rotational speed and the pressure ratio in both the compressor and turbine components, which cannot be avoided when considering the off-design performances of the system. For a certain gas turbine this is described by the compressor map and the turbine map. A sketch of these maps are shown in Figure 2.2a and Figure 4.2b, which represents the compressor map and the turbine map respectively. The mathematical representations of this relationship in the compressor are shown in Equation 2.22, 2.23, and 2.24 [43], which calculates the pressure ratio, efficiency and the required power with the input mass flow and shaft speed values.

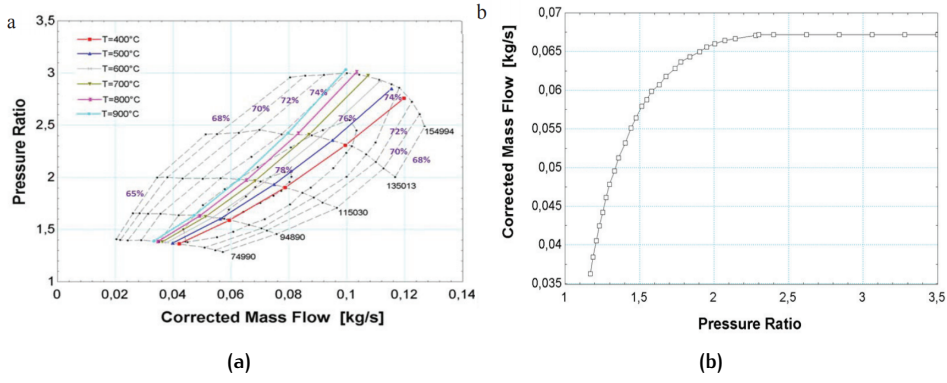


Figure 2.2: Compressor and turbine performance map of an MGT[44]

$$\pi_c = f_1\left(\frac{f_1\sqrt{T_1}}{p_1}, \frac{N_c}{\sqrt{T_1}}\right) \quad (2.22)$$

$$\eta_c = f_2\left(\frac{f_1\sqrt{T_1}}{p_1}, \frac{N_c}{\sqrt{T_1}}\right) \quad (2.23)$$

$$P_c = f_3\left(\frac{f_1\sqrt{T_1}}{p_1}, \frac{N_c}{\sqrt{T_1}}, p_1, T_1\right) \quad (2.24)$$

In reality, the detailed relationship is defined by the design of the blade shapes and the detailed layout of the compressor or the turbine system and is complicated to represent them with mathematical formulas. Numerical solutions are commonly carried out with adapting the Stodola's Law, which uses ellipse curves to represent the shape of the compressor maps. The formula is shown as Equation 2.25, notice that subscript 1 refers to off design conditions in this equation.

$$\frac{\dot{m}_0}{\dot{m}_{01}} = \sqrt{\frac{T_0}{T_{01}}} \cdot \sqrt{\frac{\pi_0^2(1 - \pi_c)^2 - (\pi_2 - \pi_c\pi_0)^2}{\pi_{01}^2(1 - \pi_c)^2 - (\pi_{21} - \pi_c\pi_{01})^2}} \quad (2.25)$$

For gas turbine systems, this is able to be simplified into the following equation:

$$\frac{\dot{m}_0}{\dot{m}_{01}} = \sqrt{\frac{T_0}{T_{01}}} \cdot \sqrt{\frac{1 - \pi_{01}^2}{1 - \pi_0^2}} \quad (2.26)$$

However, Stodola's Law only represents the performance of the compressor at a fixed shaft speed. For two-shaft gas turbines, the off design working condition are accompanied with a changing shaft speed. In order to represent this behavior, a look up table is concluded from the compressor map of the GE LM2500 gas turbine which catches up typical working points for different shaft speeds, hence introducing the following relationship:

$$\dot{m}_0 = f\left(\frac{N_c}{\sqrt{T_2}}\right) \quad (2.27)$$

Besides, the relationship between temperature, mass flow, shaft speed and the compressor efficiency is approximated by Equation 2.28, which is widely used for estimating the efficiency of turbine systems[45].

$$\eta = \eta_0 - \alpha\left(\frac{N}{N_0}\sqrt{\left(\frac{\Delta h_{s0}}{\Delta h_s}\right) - 1}\right)^2 \quad (2.28)$$

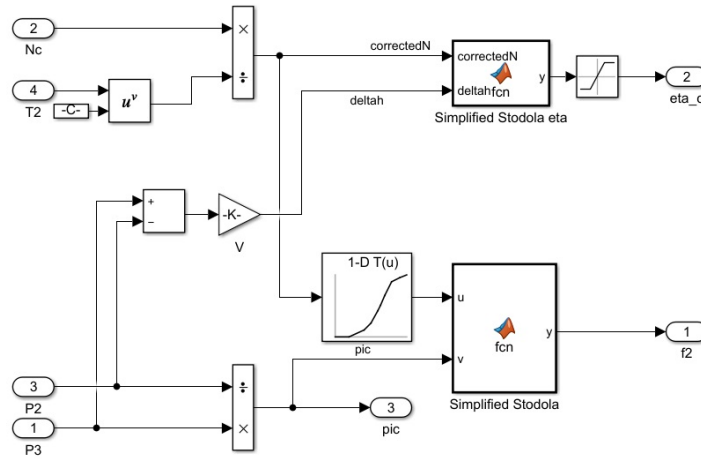


Figure 2.3: Compressor map approach block of the Simulink model.

The layout of this approximated compressor map block in the Simulink model is shown as Figure 2.3, with the equations being applied using a function block. With these calculations, the characteristics of the two-shaft simple cycle gas turbine system could be estimated. However, in order to construct a model the scale of the gas turbine also needs to be defined, and the characteristics need to be distributed into the model system.

Besides, apart from the gas turbine, in a COGAS power system there are also power being generated from the HRSG system and the steam cycle that connects to it. The power output of this additional steam cycle can be estimated with a system efficiency and the total heat flow that being sent into the system. This is shown in Equation 2.29.

$$P_{B,steam} = \eta_{td,steam} \cdot Q_{in,HRSG} \quad (2.29)$$

In this project a detailed simulation of the steam cycle is considered out of the scope and this part of the COGAS system is not going to be modeled in details. In order to have a basic estimation of the full system performance, the system efficiency of this attached steam cycle is estimated at 25% at rated power. With this estimation the performance of the entire COGAS system is able to be estimated with the power generated from the gas turbine system and the heat flow after the reheating process in the heat recovery steam cycle.

2.1.2 Scaling parameters

The scaling parameters of this gas turbine is defined to the benefit of its verification. In previous literature, Keller et al.[31] have provided static output data for an ammonia gas turbine with a total PR of 20. Other data also shows a great influence on by the factor of the total pressure ratio on TIT, specific power output and the concentration of NOx emissions[31]. In order to keep the output comparable, the total PR of the defined gas turbine is also chosen as 20, which is a reasonable value for maritime gas turbine systems. Besides, in the report Keller have also observed a relatively high TIT due to the limited amount of cooling gas[31]. This is because all the additional cooling gas needs to be provided by the EGR process to keep the equivalence ratio undisturbed. Considering this fact, the designed EGR ratio of the defined gas turbine is chosen as 0.6, which is the highest value that considered acceptable by previous researches[11][31]. The EGR ratio is defined by the following

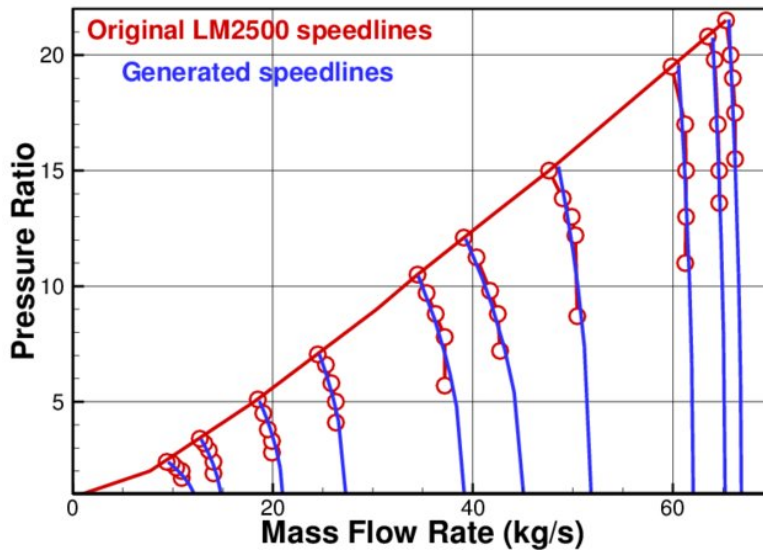


Figure 2.4: Compressor map of GE LM2500[46]

equation, with the mass of the recycled exhaust divided by the total mass of inlet air flow[31].

$$EGR = \frac{f_{EGR}}{f_{air} + f_{EGR}} \quad (2.30)$$

With the EGR ratio of 0.6, the mass flow at the designed point is chosen considering the estimated range of power output and the performance of the compressor of real gas turbine systems. Figure 2.4 shows the compressor map of the GE LM2500, with a designed air flow of 68kg/s at the pressure ratio of 18.1[17]. From this plot it is concluded that if the mass flow reduces, the designed point will shift into the surging zone, which can only be solved by introducing more compressor stages. Since the additional stages leads to a reduction of the total compressor efficiency, the designed mass flow should be kept at a large enough value with a fixed total pressure ratio.

For the defined gas turbine, the designed mass flow is chosen basing on data of several typical maritime gas turbines. With the total PR being chosen as 20, the mass flow of the compressor at the designed point is chosen as 40kg/s. This is slightly lower than the typical values, such as the one of the LM2500[17], yet larger scales may cause the full COGAS system being too powerful than the requirement of maritime usage. This observation are going be further explained in Chapter 4. The same goes for the definition of the chosen equivalence ratio of the designed point.

With the characteristics being explained and the parameters defined, the static parts of the gas turbine model are able to be constructed. But a dynamic model also requires the dynamic solvers to represent its dynamic properties. These dynamic solvers are going to be provided in the next section.

2.2 DYNAMIC CHARACTERISTICS

By definition, a dynamic model describes the components of the system that contains dynamic behaviors, which means time varying interactions among the considered variables are taken into account in the model[47]. In a lumped parameter model, the fundamental assumption is that the particular variable is assumed to be

representative for the whole control volume, which means this variable represents the average condition within this control volume. This may taken into account temperature, pressure, density, enthalpy and other variables in the processes of thermodynamic analysis. With considering the averaging conditions, the lumped parameters method further leads to the formulation of the conservation laws and constitutive equations for each control volume of the model. These equations are mostly represented using the differential-algebraic system of equations (DAEs), which is following the computational form shown as Equation 2.31[48].

$$F(t, y, \dot{y}) = 0 \quad (2.31)$$

In order to provide a more direct path for computational usage, in practice the DAEs are also able to be transformed into a system of ODEs[48], i.e.,

$$\dot{y} = G(t, y) \quad (2.32)$$

Over the years modelling of gas turbine dynamics has becoming a hot topic for researchers worldwide. Multiple methods have been created for modelling the gas turbine system for different properties. In this project, the modelling of the dynamic properties is following the method from Ying et al.[43], in which the dynamic characteristics of the gas turbine are dependent by different kinds of rotational inertias, volume inertias and thermal inertia of different components within the system.

First of all, the work fluid of the gas turbine follows the mass conservation. The changing rate of the pressure of the correlated control volumes are defined by the inlet and the outlet mass flow. This mass conservation law should be applied to the control volumes at the outlet of each component, hence the outlet of the compressor, the combustor, the outlet of the driving turbine and the outlet of the power turbine. Yet because the outlet of the compressor is the directly the combustor control volume, and the pressure loss in the combustor has been neglected in this project, these two formula has been combined. A similar case goes for the power turbine, as the outlet of this component is considered as the atmosphere, the mass conservation at this control volume has been neglected, as the outlet pressure has been assumed to be the constant value of 1 bar. The other mass conservation functions are shown as follows, with C being a constant.

$$\frac{dp_{cb}}{dt} = C_{cb} \cdot T(f_{c,out} + f_f - f_{t,in}) \quad (2.33)$$

$$\frac{dp_{t,out}}{dt} = C_t \cdot T(f_{t,out} - f_{pt,in}) \quad (2.34)$$

Besides the work fluid which follows the mass conservation laws, the driving shaft that connects the compressor and the driving turbine follows the conservation law of torque. Hence the changing rate of the rotational speed is determined by the torque requirement of the compressor and the torque delivered by the driving turbine. This is shown in Equation 2.35, which takes the driving shaft as the control volume. The other shaft that connects the power turbine and the load is considered out of the scope since the internal mechanism of the load is not considered in this project.

$$\frac{d\omega}{dt} = \frac{1}{J\omega}(G_t - G_c) \quad (2.35)$$

For the thermal conservation law, it adapts to the control volume of each component where there are chemical reactions occur, as the reaction causes additional heat input or output from the control volume. Basing on previous analysis[31], chemical

reactions are considered taking place in the combustor and the two turbine components. The compressor is considered free from chemical reactions due to the lack of reactive components in both the fresh air and the recirculated exhaust. Hence the control volumes are set for the combustor and the two turbine sets respectively. For the combustor, the changing rate of the outlet temperature is influenced by the total heat input from both air and fuel flow, the total heat output from the exhaust and the heat input due to the combustion process. Equation 2.36 shows the formula that according to this conservation.

$$\frac{dT_{TIT}}{dt} \approx \frac{\gamma R T_{TIT}}{p_{cb} V c_{p,out}} \cdot (H_{in} + \Delta H_{che} - H_{out}) \quad (2.36)$$

Similar with the combustor, energy conservation also adapts to the control volume of the two turbine stages. Yet besides the influences mentioned above, the power generated by the turbine systems are also a kind of heat outputs from the control volume, which requires to be taken into account. The formulas of these energy conservation laws are shown in Equation 2.37 and 2.38 respectively.

$$\frac{dT_{t,out}}{dt} \approx \frac{\gamma R T_{t,out}}{p_{t,out} V c_{p,tout}} \cdot (H_{tin} + \Delta H_{che,t} - H_{out} - P_t) \quad (2.37)$$

$$\frac{dT_{pt,out}}{dt} \approx \frac{\gamma R T_{pt,out}}{p_{pt,out} V c_{p,ptout}} \cdot (H_{ptin} + \Delta H_{che,pt} - H_{out} - P_{pt}) \quad (2.38)$$

Generally there are seven differential equations within this model, each is mandatory in governing the dynamic mechanisms of its control volume. With the help of these governing equations, the model is able to handle the dynamic behavior of a typical gas turbine system. But there are still several parameters in these equations that remain unknown, which has to be provided by the chemical solver systems.

2.3 CHEMICAL SOLVER

Combining the chemical model with the dynamic mechanism of the gas turbine system is the key task of this project. The simulation of chemical reactions provides the chemical heat inputs for the dynamic solvers and generates the output data of different emissions. Accuracy and credibility of the chemical model will highly define the total reliability of the final results.

From previous literature researches, it has been suggested that the thermodynamic method is sufficient for representing the chemical behavior within each component of the gas turbine system[11][31]. Different from a kinetic model, the thermodynamic model focus more on the thermal behavior of chemical reactions, and predicts the productions of the chemical process without investing into the detailed reaction rates. Calculation of chemical thermodynamics are based on the first and second law of thermodynamics, which are shown as Equation 2.39 and 2.40.

$$\Delta U_{sys} = Q - W \quad (2.39)$$

$$dQ = TdS \quad (2.40)$$

Previous researches have provided the oxidization path of ammonia at high pressure under oxidizing conditions[35]. However, for thermodynamic modelling it only focuses on the final products of the chemical reactions. In the case of ammonia

combustion, it is reported that only the following chemicals have a concentration that worth considering in the products of ammonia combustion: H₂, O₂, N₂, H, O, OH, HO₂, H₂O, H₂O₂, NH₃, N₂O, NO, and NO₂[31]. However, for the atomic oxygen (O) there have been little published data on its thermochemistry properties over different temperatures, and since this report will focus on the fuel-rich combustion processes, there will be few chances for this strongly oxidizing chemical to concentrate in the exhaust. Following this guidance it is considered that there are 13 different chemicals being considered in this project, with Ar being added representing its concentration in fresh air and O being neglected due to the preceding reasons. For the calculation of the thermodynamic properties, a set of polynomial equations are used in this project for calculating the heat capacity, enthalpy and entropy of each chemical with sets of coefficients provided on the NIST website[9]. The equations are shown as the followings:

$$c_p = A + Bt + Ct^2 + Dt^3 + E/t \quad (2.41)$$

$$H - H_{298.15} = At + \frac{1}{2}Bt^2 + \frac{1}{3}Ct^3 + \frac{1}{4}Dt^4 - E/t + F - H \quad (2.42)$$

$$S = A \ln(t) + Bt + \frac{1}{2}Ct^2 + \frac{1}{3}Dt^3 - \frac{1}{2}E/t^2 + G \quad (2.43)$$

The NIST data sheet for the considered chemicals are included in the Matlab code in Appendix I of this report.

To predict the concentration of each chemical after reactions, a common method of minimizing the Gibbs free energy is applied in this project for the combustion and expansion processes of the gas turbine according to previous experiences[31]. Gibbs free energy is the energy associated with a chemical reaction that can be used to do work, and is defined as shown in Equation 2.44.

$$\Delta G = \Delta H - T\Delta S \quad (2.44)$$

The reaction is considered spontaneous if the Gibbs free energy is negative, and nonspontaneous if it is positive. By minimizing the Gibbs free energy, this chemical thermodynamic calculation predicts the final production of the selected chemicals under defined input condition values. This is accompanied by the output data of enthalpy difference and the contribution of this chemical process to the temperature of the fluid mixture. With these values being generated it is able to provide the required inputs of the conservation functions which have been mentioned in the previous section. Besides, it is worth of mentioning that this method is adapted basing on conclusions of precious kinetic analysis that the combustion process is able to be finished fast enough.

In the modelling practice, minimizing the Gibbs free energy requires the adaptation of the `fmincon` function provided by Matlab toolbox. However, this non linear solver is out of the range from what is able to be solved by the Simulink tool. In this condition, the chemical model is provided in the form of Matlab code, using the `fmincon` solver to minimize the Gibbs free energy and an additional `fzero` solver to find out the ending temperature of the system. Three identical sets of this code are created for the combustor, the driving turbine and the power turbine component respectively, and being called by the Simulink model with a `coder` function. From later testing a forth set of the code is also created for representing the combustion process in the reheat boiler of the COGAS system. The code set for the combustor is listed in Appendix I.

With all the required tools being provided, the model is able to be assembled using the Simulink software. The layout of the system is going to be provided in the next section.

2.4 SYSTEM LAYOUT

In the previous sections, all the required governing functions for the characteristic of the gas turbine model have been provided. This section is going to explain on the detailed layout of the different functions in the Simulink model. A general view of the simulation model is provided in Appendix II of this report.

2.4.1 EGR block

On the general basis, the ammonia gas turbine model is divided into seven main components. The EGR block, of which the format is backgrounded green takes control of the EGR ratio and mixes the recirculated exhaust with fresh air. This block receives the chemical distribution of the condensed exhaust gas, and delivers the chemical distribution of the inlet work fluid with its inlet temperature and pressure.

2.4.2 Compressor

The first component of the gas turbine model is the compressor block. This block receives the signal of inlet chemical components, the inlet temperature, both inlet and outlet pressure and the rotational speed of the driving shaft. On the other hand it generates out the mass flow that passes through the compressor with its outlet temperature and the required torque of the compressor blades. There are 3 different formulas included in this block. The compressor map generates the mass flow that passes through this component and the efficiency of the compressor stages. These signals are used in the next sub-block to calculate the temperature ratio of this stage.

With the outlet temperature being calculated, the power required for driving the compressor is able to be calculated with Equation 2.9 in Section 2.1.1. The required torque is generated with the power requirement and the shaft speed. The general layout of the compressor block is shown in Figure 2.5.

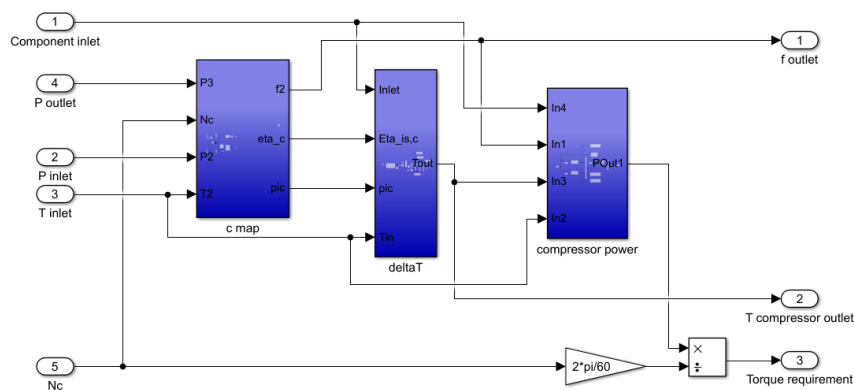


Figure 2.5: Layout of compressor block

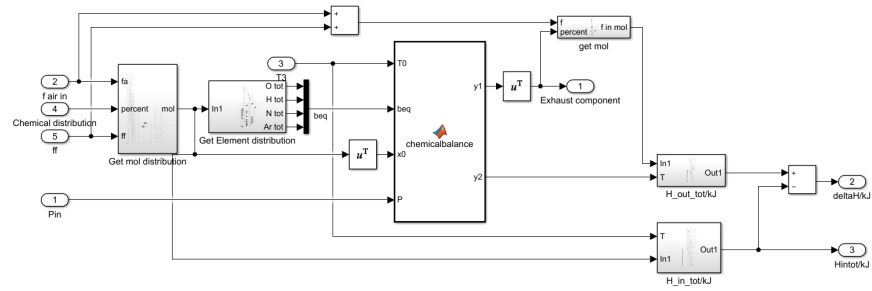


Figure 2.6: Layout of chemical model block

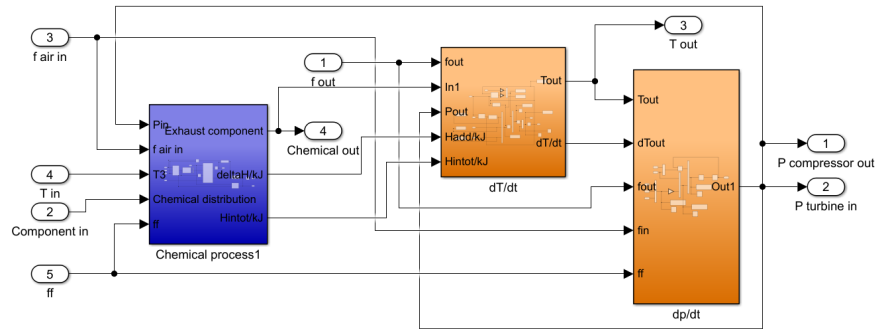


Figure 2.7: Layout of combustor block

2.4.3 Combustor

The combustor block represents the real combustor of the gas turbine system. It receives the signal of work fluid mass flow inlet and outlet of this component, the mass flow of fuel injection, the inlet temperature and the chemical distribution of the work fluid. What is sent from this block is the inlet and outlet pressure of the work fluid, the inlet and outlet temperature and the chemical distribution of the work fluid after the combustion process. Four sub-blocks are included in this component. The first one represents the chemical process. The signals data of fuel and inlet air flow is mixed and sent into the chemical solver. Results of the chemical equilibrium is used to calculate the enthalpy difference that caused by this chemical process. The distribution of this sub-block is shown as Figure 2.6.

Besides the chemical block, there are also two different conservation solvers in this component. One is the energy conservation for the combustion chamber, following Equation 2.34 in Section 2.2. The other is the mass conservation for the compressor outlet, which is also the combustion chamber volume. This block follows Equation 2.31 in 2.2.

The distribution of this component is shown in Figure 2.7.

2.4.4 Driving Turbine

This block represents the high pressure turbine of the real gas turbine system, which supplies the power that required by the compressor. In this model, it receives the signal of inlet and outlet pressure of this component, the turbine inlet temperature, the rotational speed of the driving shaft and the chemical distribution of the work fluid. On the other hand, this block delivers the mass flow that pass through the turbine component, the outlet temperature and chemical distribution of the work fluid, and the torque being generated by the turbine stages for driving the compres-

Besides the chemical reactions, there are also characteristic solver in this component. Like the compressor map for the compressor system, the turbine also have its turbine performance map. The turbine map of the high pressure turbine is usually calculated from the compressor map that it needs to match. The matching principles include the matching of shaft speed, mass flow and the balancing on power. Due to the same reason being mentioned in Section 2.4.2, the same method is used to generate the approximation of the turbine map. Following the turbine map and the adaptation of Equation 2.27, this block generates the mass flow that passes through the high pressure turbine component and the turbine efficiency.

Due to the presence of chemical reactions, the control volume of this high pressure turbine also follows the conservation law on energy. This dynamic solver is constructed following Equation 2.35 and calculates the outlet temperature of the high pressure turbine.

With the data signals provided above, it is able to calculate the power being generated by the high-pressure turbine using Equation 2.13. This calculated power delivery is then converted to the torque that being sent to the driving shaft. The general insight of this block format is shown as Figure 2.8.

Despite what is considered inside the block format, there is also a dynamic conservation function being adapted to govern the mass conservation at the outlet of this high-pressure turbine sets. This block is constructed following Equation 2.32 and governs the outlet pressure of the working fluid at the turbine outlet. The distribution of this block is shown in Figure 2.9, which also shows how this formula is connected with the main format of this high-pressure turbine component.

2.4.5 Power turbine, shaft and additional components

Due to the identical working principles, the block of the power turbine has a similar distribution with the high pressure driving turbine which is shown in Section 2.4.4. The only difference is that this component works at a lower inlet pressure which is exactly the outlet of the driving turbine, and what this component delivers is the output power to drive the load. Basing on these working principles, the shaft speed of this stage is set to a constant value of 3 600 rpm, which is able to lead to a power generator delivering AC power at either 50Hz or 60Hz. The outlet pressure is also considered as the constant atmosphere pressure of 1 bar.

Besides the main components of the gas turbine system, there are also several other components in this Simulink model. One of the most important one is the driving shaft that connects the compressor and the high pressure turbine. The momentum conservation equation of Equation 2.33 is used to represent the dynamic behavior and controls the rotational speed of this driving shaft. With the signal of torque requirement and delivery, this block generates the shaft speed to both the compressor and the high pressure turbine.

Despite the previous components that forms the gas turbine system, another block is attached for the EGR process. Basing on previous literature analysis, it is considered that the recirculated exhaust gas should be condensed to the inlet temperature of the compressor, which would be beneficial to reduce the power requirement of the compressing process. This, however, influences the chemical distribution of the recirculated exhaust, because there is high concentration of water vapour in the exhaust which has been condensed into water during this process. Hence an additional block is attached to represent this process, and filters away the water concentration in the recirculated exhaust. An insight of this filter is shown in Figure 2.10.

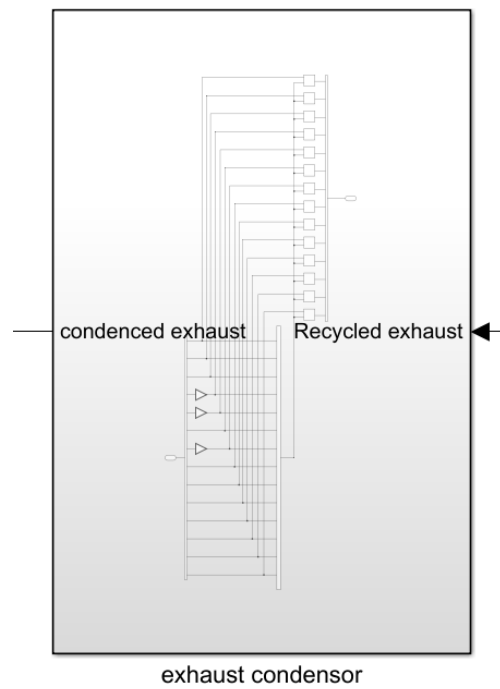


Figure 2.10: Outside look of condensing block

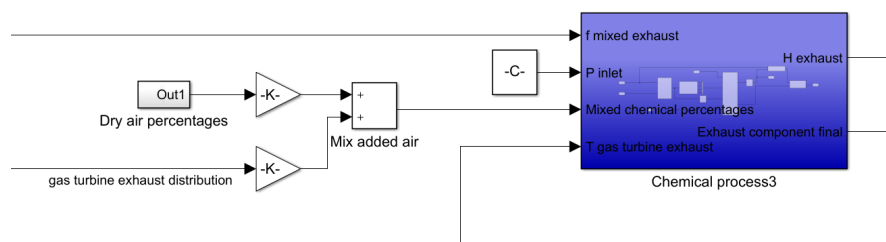


Figure 2.11: re-heater

Additionally, during testing of this model, it is found that the chemical reactions in the reheating process of the boiler cannot be neglected for estimating the NO_x emission of this COGAS system. Hence an additional set of chemical solver block is attached to represent the chemical processes in the **hesg!** (**hesg!**) re-heater. In this block, it is considered that the concentration of hydrogen in the exhaust of the gas turbine is combusted at the situation of a chemical equilibrium, hence an equivalence ratio of 1.0. The distribution of this additional block is shown as Figure 2.11. This block provides the total enthalpy that sent into the system, which is the total heat input that received by the heat recovery steam cycle.

A general view of the full Simulink model of this ammonia gas turbine system is attached as Appendix II.

2.5 CHAPTER SUMMARY

In this chapter, a dynamic model combining the chemical mechanical properties of an ammonia gas turbine system is constructed. The general ideas of this model is provided including the characteristics of gas turbine system, the differential equa-

tions for governing the dynamic behaviors, and the thermodynamic methods to represent the chemical behaviors of the working fluid. The scale of the gas turbine system is defined basing on previous researches and its adaptation for maritime usage. These theories are then used for the modelling process in the Simulink tool.

With the model being constructed, testings can be done to verify the system before it is able to be used on solving the research questions. The verification process is going to be provided in the following chapter.

3

STATIC MODEL VERIFICATION

Verification is a process to determine whether the model represents the mathematical model and its solution accurately. The model has to be verified before it is able to be used for further researches. Even though the model is not able to be validated with data collected from practices due to a lack of experiment results, comparing the output with numerical calculation and results from previous simulations are still able to provide a verification to this model and examine its reliability.

For complex models which consists many sub-systems, it is suggested to verify each of the sub-systems separately before connecting these components together[49]. Considering the model of this project, the chemical solver is an additional attachment to the dynamic model of the gas turbine. Besides, the compressor and turbine maps being used by this model are estimated basing on a simplified method. The performance of these sub-systems needs to be checked first before verifying the complete model.

3.1 VERIFICATION OF THE CHEMICAL MODEL

In Section 2.3, it has been mentioned that the chemical solver of this model is constructed basing on the chemical thermodynamic theory of minimizing the system Gibbs free energy. Basing on this method, the model should be able to provide the correct outputs of the considered chemical mixture when it reaches its chemical balance after the reaction processes. In order to verify this model, the output of this chemical solver is compared with the results of previous analysis that provided by Keller et al.[31].

In his evaluation analysis on the ammonia COGAS power system, Keller used the same method of minimizing system Gibbs free energy with the CHEMKIN software, and provided data of the turbine inlet temperature under variant condition sets[31]. By comparing the turbine inlet temperature calculated with identical condition settings, it is able to define whether the chemical model constructed for this project is made in the correct way. The comparing results are shown in Figure 3.1, in which the red dots are the results generated by the Simulink model of this project. These data sets from the Simulink model are provided without implementing the EGR process and the pressure ratio is fixed at 20. These are the same settings as those adapted by the black and gray curve from Keller's measurement[31]. The equivalence ratios are set as what is distributed in the plot from 0.5 to 1.5 respectively.

From this figure, it is noticeable that the red dots calculated by the Simulink model of this project matches well with the data from previous analysis. A little difference has been observed between the two sets of data yet is explainable by the different chemical database being introduced in the two projects. This result indicates that the chemical model is able to generate correct data with its constructions, hence it is confident to say that the chemical model of this project is correctly constructed.

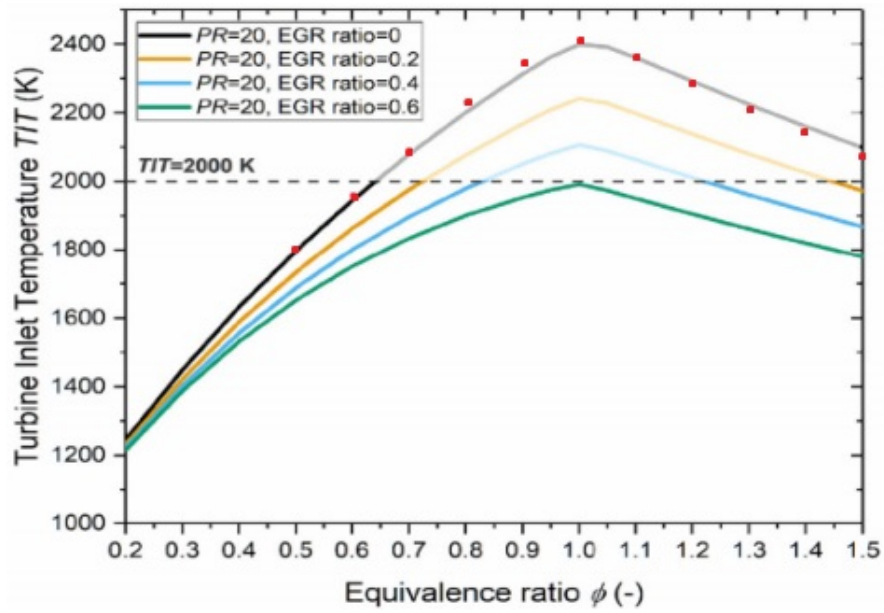


Figure 3.1: Comparison of calculated TIT with previous research[31]. PR=20, EGR=0, with red dots being data generated by the chemical solver.

3.2 VERIFICATION OF COMPRESSOR AND TURBINE MAPS

As mentioned in Section 2.1.1, both the compressor and turbine maps are constructed with a simplified method due to data installing issues with the Simulink look-up table block. The simplified ellipse law is used to represent the behavior under different pressure ratios, hence only the influence of shaft speed is concluded from the data of a real compressor system. The same goes for the efficiency, as both the compressor and turbine efficiencies are following the same method that is shown in Equation 2.33. These adopted methods have to be verified to make sure that these blocks are constructed correctly.

To ensure that the model is correctly built, these compressor and turbine blocks should have a same qualitative behavior as what a real map provides. For instance, with the shaft speed remaining unchanged, a lower pressure ratio will result in a slightly higher mass flow in the compressor, yet the efficiency of the system will observe a decrease. Basing on this method, several tests of this kind are provided for all the three map blocks within the model basing on the characteristics of the real systems. The results of the compressor map, the driving turbine map and the power turbine map are shown in Table 3.1, 3.2 and 3.3 respectively.

Table 3.1: Verification results of the compressor block.

Compressor						
Action	Involved signal	Expected behavior	Actual output before	Actual output after	Actual behavior	Match or not
Reduce shaft speed	mass flow	↓	40.0kg/s	30.0kg/s	↓	Y
	efficiency	↓	82.0%	81.1%	↓	Y
Increase outlet pressure	efficiency	↑	59.6%	83.8%	↑	Y
Increase inlet temperature	mass flow	↓	40.0kg/s	25.7kg/s	↓	Y

Table 3.2: Verification results of the high-pressure turbine block.

Driving turbine						
Action	Involved signal	Expected behavior	Actual output before	Actual output after	Actual behavior	Match or not
Reduce shaft speed	mass flow	↑	44.0kg/s	46.0kg/s	↑	Y
	efficiency	↓	87.0%	86.1%	↓	Y
Increase outlet pressure	mass flow	↑	44.0kg/s	44.1kg/s	↑	Y
	efficiency	↓	87.0%	86.9%	↓	Y
Reduce inlet pressure	mass flow	↓	44.0kg/s	31.8kg/s	↓	Y
	efficiency	↓	87.0%	83.7%	↓	Y

Table 3.3: Verification results of the power turbine block.

Power turbine						
Action	Involved signal	Expected behavior	Actual output before	Actual output after	Actual behavior	Match or not
Reduce inlet temperature	efficiency	↓	89.0%	86.9%	↓	Y
Reduce inlet pressure	mass flow	↓	40.0kg/s	23.9kg/s	↓	Y
	efficiency	↓	89.0%	74.8%	↓	Y

From these tables, it is able to conclude that all three map blocks have provided a similar behavior as from the real system. This means that these blocks are able to represent the characteristics and behaviors of the real systems, and hence be considered as verified.

With the sub-systems being verified, it is able to provide the verification process of the full gas turbine model system.

3.3 VERIFICATION OVER COMPLETE SYSTEM

Since the model is dynamics, it should be verified under both static and dynamic conditions. However, due to its fuel-rich working conditions and the relatively high system complexity, the dynamic behavior of such a gas turbine system is affected by many factors and hard to examine. During the test of this model, some odd behaviors have been observed from the model and prevents further analysis of the dynamic behaviors. This will be discussed in details in Chapter 5 of this report. In this section only the static performance is verified with comparing the static outputs under designed point with the results of numerical calculations.

In order to verify the static output, different parameters generated by the model under its designed point is compared with numerical results. Table 3.4 shows the comparison of several random parameters from the model output and the results from numerical calculation. The total pressure ratio of the compressor is 20, with the high-pressure turbine is calculated to fulfill the requirement of delivering the power that required by the compressor. Notice that the efficiency of the compressor, high-pressure turbine and power turbine at the designed point are defined as 82%, 87% and 89% respectively. These are relatively conservative values which are selected basing on fact that this gas turbine has a relatively high pressure ratio

Table 3.4: Comparison of numerical calculation and model outputs at designed point.

Parameter	Numerical result	Model result
Compressor required power (MW)	20.80	20.99
Compressor outlet temperature (K)	790.29	789.60
Driving turbine PR	4.16	3.51
Driving turbine outlet temperature (K)	1188.65	1207.00
Power turbine PR	4.81	5.69
Exhaust temperature (K)	840.27	842.70
Gas turbine power output (MW)	20.51	25.80

comparing with a relatively low air mass flow, hence more shaft stages would be required for preventing surging at a trade-off of the efficiency. Besides, for numerical calculations, the c_p of inlet mass is assumed to be constant at the value of 30J/mol.K, with the isentropic constant being fixed at 1.4. The same goes for the exhaust, with the c_p assumed constant at 33.5J/mol.K, and the isentropic constant at 1.33.

From Table 3.4 it is concluded that most of the numerical data are comparable with that from the model output, only except for the point of the high-pressure turbine outlet. However, this is able to be explained by the variable c_p being adapted in the Simulink model, which is better matching the real condition that the c_p of the exhaust components are increasing as temperature builds up. With the variable c_p , the exhaust is able to deliver more heat with a lower pressure loss comparing with the constant situation, hence resulting in the difference of the matching point.

With the difference of the high pressure turbine matching point being explained and decided to be acceptable, it is able to consider that the output of the model is matching well with numerical calculations. Hence it is able to say that the model is verified on the static level.

3.4 CHAPTER SUMMARY

In this chapter, verification process is provided over different blocks and the over all level of the model. As the newly implemented parts, the chemical solver is verified with the data from previous analysis. The compressor and turbine maps are verified by comparing the qualitative behavior due to the simplification methods attached because of practical issues. Then with these components being verified, the whole model is verified against numerical calculations to examine its static performance at the designed working condition. The results shows that the output data of the model matches the numerical results with little difference, hence the model is considered correct for its static outputs. Further analysis over the dynamic performance is going to be provided and examined in Chapter 5 of this report.

With the model being generally verified, it is considered that the model is able to be used for answering the research questions of this project. The analysis over its static performance under off design conditions are going to be provided in Chapter 4. A further looking into the dynamic performance and special concerns over the controlling of such systems will be further examined and explained in Chapter 5.

4

STATIC PERFORMANCE OF THE AMMONIA GAS TURBINE

During its operation, a gas turbine system will usually not work at rated power. This is particularly common for maritime power systems as the power requirement of the ship is highly dependent on its speed and maneuvering processes. In the introduction, it has been stated that there has been a lack of understanding on the off design performances of the gas turbine system which is designed for running on ammonia fuel. In this chapter, both the design and off design working performances of the ammonia gas turbine system are going to be examined with the Simulink model.

First of all, the detailed design parameters of the gas turbine system are further defined and explained in Section 4.1. This is provided together with a brief analysis on the performance of the designed gas turbine system at its designed working condition. Following that, different part load conditions are examined on a basis of different fuel flow injection ratio. Section 4.2. shows the matching process of the high pressure turbine map over these part load conditions and puts a general overview on the off-design performances of the modeled system. To answer the research questions of this project, Section 4.3 discusses the power output and efficiencies over these part load conditions, and a further look is taken into the emission ratio of these off-design points.

4.1 DESIGN POINT OF THE GAS TURBINE

Before zooming into the off-design points, the rated working condition of this gas turbine system needs to be determined. In Section 2.1.2, the gas turbine system has been designed with a total pressure ratio of 20 and a compressor mass flow of 40kg/s. An EGR ratio of 0.6 has also been chosen basing on previous literature. However, in order to define the complete working condition, the fuel injection ratio also needs to be chosen before it is able to calculate the power and other performances.

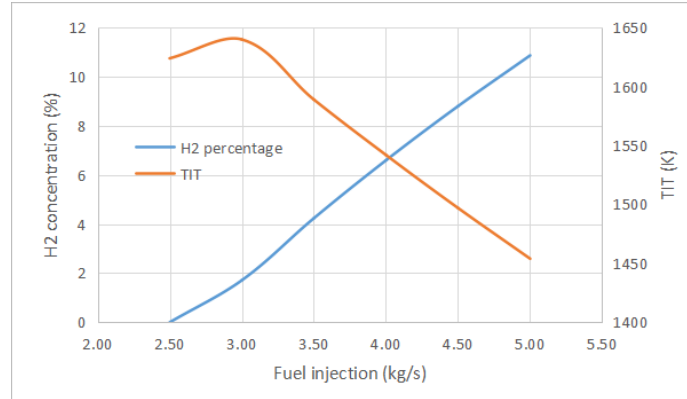
4.1.1 Defining fuel injection

With the current settings, the mass flow of fuel injection directly leads to the equivalence ratio of the combustion process. A higher equivalence ratio leads to a higher H₂ concentration in the exhaust and a slightly lower turbine inlet temperature[31]. Previous experiments basing on a MGT system has suggested an equivalence ratio of 1.1 considering NO_x emission and un-burned ammonia[16]. However, for larger gas turbine systems which have a higher pressure ratio, a higher concentration of H₂ is generated from un-burned ammonia, makes this product unable to be ignored[11]. It has been suggested that this H₂ concentration can be combusted in the HRSG of the COGAS system. Yet this would require the H₂ concentration being high enough to be combusted.

It is stated that for a H₂-N₂ mixture, which is a good representative of the gas turbine exhaust, the molar concentration of H₂ needs to be higher than 5.5%[50]. This would be even higher considering that water vapour is also presenting in the

Table 4.1: H₂ concentration and TIT with different fuel injections.

Fuel flow (kg/s)	H ₂ (%)	TIT (K)
2.50	0	1624
3.00	1.711	1640
3.50	4.239	1589
4.00	6.598	1542
4.50	8.804	1497
5.00	10.87	1454

**Figure 4.1:** H₂ concentration and TIT with different fuel injections.

exhaust mixture. Hence in this project it is suggested to have the H₂ concentration timed by an additional 1.1 factor. Besides, as a higher turbine inlet temperature will benefit the thermal efficiency of the gas turbine system, it is considered that as long as the H₂ concentration limit is fulfilled, a higher TIT would be preferable.

Following these limits, the model is tested over different fuel injection ratios. Table 4.1 shows the TIT and H₂ concentration over a fuel injection mass flow from 2.5kg/s to 5kg/s, which is also plotted in Figure 4.1. From the table it can be noticed that with a fuel flow of 4 kg/s, there is a hydrogen concentration of 6.62% with the TIT being at 1542K, which fulfills the H₂ concentration limit as well as providing a reasonable TIT for the designed gas turbine system. This, however, results in a high equivalence ratio of 1.49, much higher than the suggestion from previous researches[16]. Since the chemical model in this report is constructed basing on chemical balancing calculations, it is not able for this project to define how completely the additional ammonia is cracked into hydrogen under this designed condition. To answer this question there will be a further need in chemical kinetic analysis. For this project, it is going to apply the assumption that the chemical balance is able to be reached. This is based on the conclusions from Okafor et al.[11] and Keller et al.[31] while also considering that the experiment is based on a low pressure ratio MGT with a significantly lower peak temperature around 1100K[16].

4.1.2 System performance at designed point

At this stage, all the design parameters for the gas turbine model has been defined. It is now able to provide the performance data of this modeled gas turbine system under its designed point. A partial set of data output of this gas turbine system under the designed point has been shown in Table 3.4, which have been used for the verification of this model in Chapter 3.

With a mass flow of 40kg/s and a fuel flow of 4kg/s, this ammonia gas turbine

system is able to generate a power output of 25.8MW, which is comparable with the RR WR21 and GE LM2500+ gas turbines which both have a much higher air mass flow, and is significantly higher than the GE LM1600 system of which the air mass flow is comparable[17][39]. This is due to the fact that the additional gas, which is EGR gas for this ammonia gas turbine system and additional fresh air for traditional gas turbines, takes a much lower percentage of the compressor mass flow for this designed gas turbine system. Hence with a smaller air mass flow there are more fuel to be combusted, resulting in a higher specific power of the system. This high specific power can lead to a reduction of the total weight and volume of the COGAS power system, hence further increases its advantage over traditional diesel system or diesel hybrid systems.

Yet despite having a higher specific power, the system efficiency of the ammonia gas turbine is slightly lower than that of current gas turbine systems. At the rated working point with 25.8MW power output from a 4kg/s ammonia fuel flow, the system efficiency is 34.68%, comparing with the efficiency of an GE LM2500+G4 DLE being able to achieve 38.5%[17]. However, this does not mean the ammonia gas turbine is lack of competitiveness, but due to the fact that this system keeps a very high equivalence ratio to generate a high enough H₂ concentration in the exhaust to make it combustable in the HRSG re-heater system. Under its designed working condition, with an exhaust temperature at 842.7K at power turbine outlet, the temperature after the reheating process is able to reach 1265K, leaving a heat flow of more than 60MJ/s at the inlet of the heat recovery steam cycle. With the efficiency of this heat recovery steam cycle being estimated at 25% in Section 2.1.1, the steam cycle is able to generate an additional power output of 15.2MW, resulting in a total power output of 51MW and a system efficiency of the COGAS being 54.87%. This is comparable with the GE LM2500+G4 COGAS system which has a system efficiency between 54.6% and 55% with different system layouts[17]. Hence for the complete system, it is able to conclude that the ammonia COGAS system is able to have a comparable performance with the current COGAS systems and is able to maintain the advantages over other power systems under an ammonia economy when adapted for maritime usage.

Table 4.2: Data output for the designed point of the ammonia gas turbine model.

Fuel injection (kg/s)	4.0
Compressor mass flow (kg/s)	40.0
Compressor PR	20.000
Compressor efficiency (%)	82.00
Compressor outlet temperature (K)	789.6
Shaft speed (rpm)	9600
TIT (K)	1542
High pressure turbine PR	3.514
High pressure turbine efficiency (%)	87.00
High pressure turbine outlet temperature (K)	1207
Power turbine PR	5.692
Power turbine efficiency (%)	89.00
Exhaust temperature (K)	842.7
Gas turbine power output (MW)	25.80
Gas turbine system efficiency (%)	34.68
NO _x emission (ppm)	9.161
NO _x emission (g/kWh)	0.0652
NO _x emission (g/kg.fuel)	1.169E-04
Re-heat HRSG temperature (K)	1267
H ₂ concentration in GT exhaust (%)	6.617
HRSG heat flow (MJ/s)	60.08

In this section, the last design parameters of the gas turbine system is defined, and the system performance at designed point is concluded and evaluated basing on the power output and system efficiency. The full set of data output for this designed working condition is shown in Table 4.2.

4.2 OVERVIEW ON OFF-DESIGN PERFORMANCE

For two-shaft gas turbines, the additional shaft provides the ability to run the gas turbine system more effectively. By shifting the shaft speed, the compressor and high pressure turbine system are able to keep a high efficiency over different loading conditions. In this project, it is defined that the combustor will be kept under a constant equivalence ratio, this is to ensure that the H₂ concentration in the exhaust is kept high enough to be combusted in the HRSG, while the TIT is kept at a high level for a higher part load thermal efficiency.

Basing on these rules, the part load performance of the ammonia gas turbine system is calculated over different fuel injection ratio from 100% to 40%. The basic output data sets are provided in Table 4.3, with the full table being attached as Appendix III.

Table 4.3: Data output for different fuel injections of the ammonia gas turbine model.

Fuel injection (kg/s)	4.0	3.6	3.2	2.8	2.4	2.0	1.6
Fuel injection ratio (%)	100	90	80	70	60	50	40
Compressor air flow (kg/s)	40.0	36.0	32.0	28.0	24.0	20.0	16.0
Compressor PR	20.00	17.42	15.47	13.22	10.89	8.95	6.71
Compressor efficiency (%)	82.00	80.61	78.50	74.97	69.96	64.23	55.80
TIT (K)	1542	1519	1505	1490	1475	1464	1448
High pressure turbine PR	3.514	3.390	3.368	3.410	3.535	3.751	4.175
HT efficiency (%)	87.00	85.61	83.61	80.42	76.09	71.24	64.26
HT outlet temperature (K)	1207	1202	1200	1196	1192	1191	1187
Power turbine PR	5.692	5.138	4.594	3.877	3.081	2.386	1.607
PT efficiency (%)	89.00	88.69	85.77	84.95	79.32	70.75	52.86
Exhaust temperature (K)	842.7	857.6	879.3	915.3	969.2	1033	1120
GT power output (MW)	25.80	21.98	18.24	14.02	9.58	5.70	1.95
GT system efficiency (%)	34.68	32.83	30.65	26.92	21.47	15.32	6.56

With these output sets, a further analysis is made over the TIT, pressure ratio, power output and the thermal efficiency of both the gas turbine system and the combined COGAS system.

4.2.1 Turbine inlet temperature

Figure 4.2a shows the TIT over different fuel injection ratios from 40% to 100%. With the fuel injection percentages growing, the TIT also increases slightly from 1448K at 40% fuel injection to 1542K under full load. This has been due to the difference of the compressor outlet temperature over different working conditions. From ?? it can be seen that the TIT increase is parallel to that of the compressor outlet temperature, which is able to be further explained by the fixed equivalence ratio. With the equivalence ratio being fixed, the chemical balance of the combustion process have

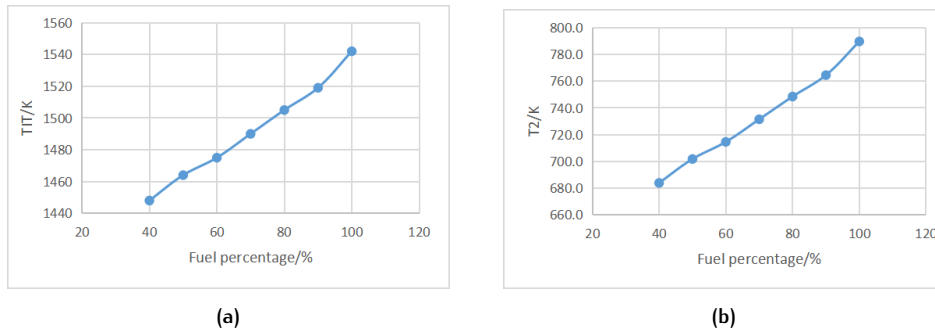


Figure 4.2: TIT and compressor outlet temperature (T_2) of the gas turbine over different fuel injection ratios.

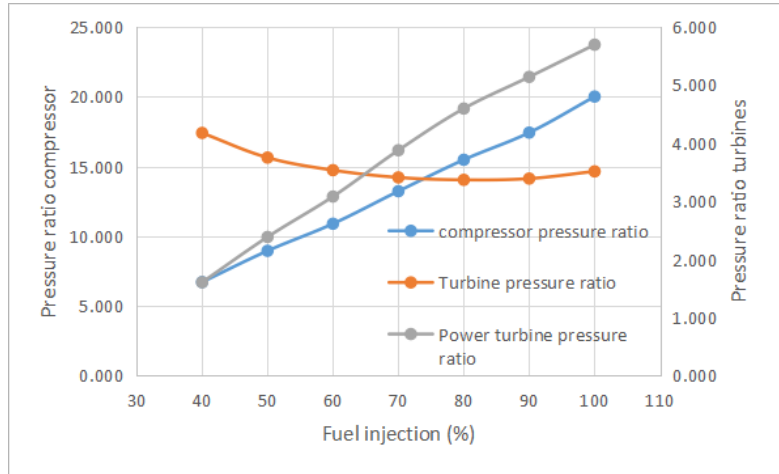


Figure 4.3: H₂ concentration and TIT with different fuel injections.

little difference over different pressure ratios, leading to an almost fixed temperature increase in the combustor.

Yet despite the slightly difference of TIT, it has little influence on the part-load performance of system efficiency and exhaust, which are to be discussed in the following sections.

4.2.2 Pressure ratios

There are three pressure ratios considered in this project, the pressure ratio of the compressor, the high-pressure turbine and the power turbine. The outputs over fuel injection ratio is shown in Figure 4.3. From the output, both pressure ratios of the compressor and power turbine decreases dramatically as the fuel flow ratio decreases. This can be explained by the dramatic decrease of the air mass flow requirement. However, the pressure ratio of the high pressure turbine shows a different behavior. As the fuel injection ratio decreases, the pressure ratio first decreases slightly from 100% fuel injection to 80%, then begins to increase from 80% fuel injection to 40%.

The odd behavior of the high pressure turbine is able to be explained with two different reasons. Firstly, when the fuel injection decreases, the requirement of air mass flow also decreases, which also leads to the drop of the pressure ratio of the compressor. Since the compressor is driven by the high-pressure turbine via the driving shaft, the power delivered by the high-pressure turbine is dependent on the compressor's requirement. With the power requirement of the compressor drops

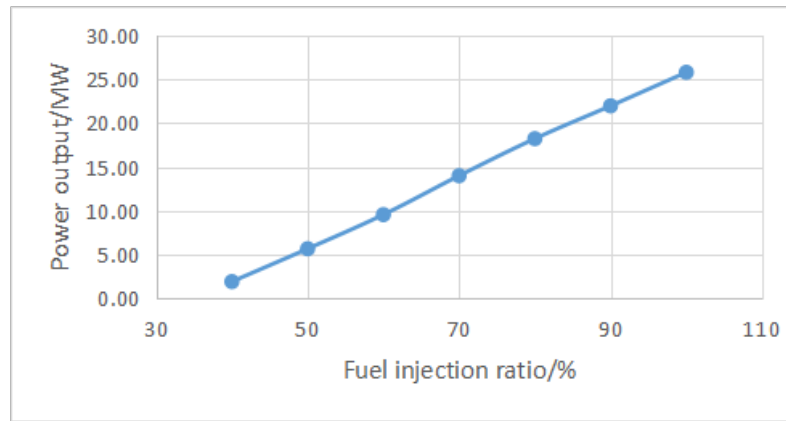


Figure 4.4: Power output of the gas turbine against fuel injection ratios.

more sharply than the mass flow itself, the high-pressure turbine also requires a lower pressure ratio to fulfill this power requirement. However, when the mass flow becomes too low, the efficiency of both the compressor and the turbine system drops significantly. Hence there would be more specific power requirement to compress a certain mass flow with a certain pressure ratio. From the output it can be noticed that with fuel injection ratio dropping from 100% to 40%, the efficiency of the compressor and the high pressure turbine drops from 82% and 87% to 55.80% and 64.26% respectively. This has been a more significant difference than the dropping of compressor pressure ratio. Hence the high-pressure turbine has to take a higher pressure ratio to deliver the required power of the compressor component.

4.2.3 Power and efficiencies

The power out distribution of the ammonia gas turbine against the fuel injection ratio is shown in Figure 4.4. From the plot it observes a linear relationship between the power output and the fuel flow injection. However, with the fuel injection decreases from 100% to 40%, the power output of the gas turbine system drops more significantly from 100% to just 7.57%. This is caused by the decrease of the efficiency of all the three turbine components of the system, with the compressor efficiency dropping from 82% to 55.80%, the high-pressure turbine efficiency from 87% to 64.26%, and the power turbine from 89% to 52.86%. These dropping in system efficiency causes a significant decrease in the pressure ratio of the power turbine system, from 5.692 at 100% fuel injection to 1.607 at 40%. Under these part load conditions, most of the total pressure ratio has been used to cover the power requirement of the compressor, leaving little for delivering the output power. This can also be revealed from the exhaust temperature. With the fuel injection ratio dropping, the exhaust temperature increases from 842.7K at full load to as high as 1120K with a 40% fuel injection, making the system efficiency of the gas turbine dropping from 34.68% to as low as 6.56% at 40% fuel injection. The system efficiency over different part load conditions are shown in Figure 4.5.

Luckily, for the complete COGAS system, the heat in the high temperature exhaust is able to partly recovered by the HRSG system. With a higher exhaust temperature, the efficiency of the HRSG is able to increase, since the exhaust temperature after the reheating process is able to reach as high as 1559K and leads to a heat flow of 32MJ/s to the HRSG, which is more than half of the heat flow under the full load condition. Considering a part load efficiency of 12.5% for the HRSG system, it will lead to a part load efficiency of the COGAS system at 20.98%, which is significantly higher than the gas turbine efficiency itself.

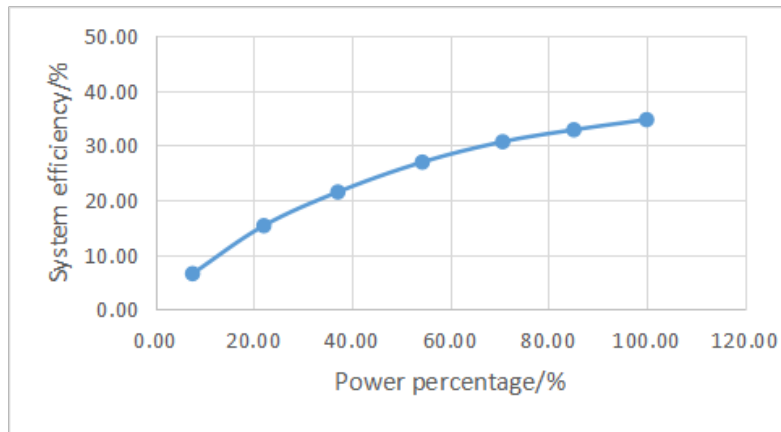


Figure 4.5: System efficiency of the gas turbine against fuel injection ratios.

All in all, basing on the current settings, the ammonia gas turbine shows a similar behavior with traditional gas turbine systems under part loading conditions. As the fuel injection ratio decrease, the total pressure ratio decreases sharply while the TIT also decreases slightly due to the slightly drop on compressor outlet temperature. A faster drop on the power output is observed with the fuel injection ratio decreases, which has been caused by the decrease of power turbine pressure ratio and further due to the decrease of total pressure ratio and the efficiencies of compressor and turbine components. Low part load efficiency has lead to an increase of exhaust temperature, which on the other hand provides a positive affect on the HRSG system. Even though part load efficiency of the gas turbine drops dramatically, the efficiency of the complete COGAS system may decrease much more slowly.

4.3 DISCUSSION ON EMISSIONS

Performance of the gas turbine system over emission factors have been a key topic of this project. The chemical model is constructed to answer the research questions on the emission of the gas turbine system over its off-design conditions. By testing the model over different fuel injection ratios, the thermal chemical performance is also observed from the Simulink model of the ammonia gas turbine system.

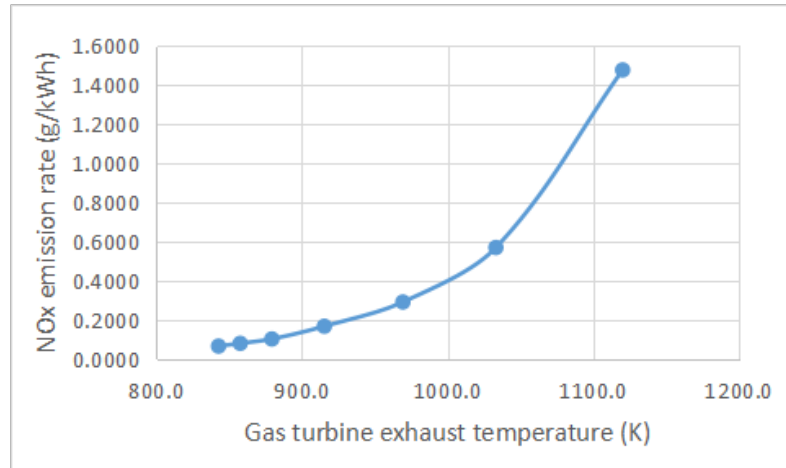
However, since the chemical model of this project has been based on calculation of chemical balances, the chemical reaction in each component of the gas turbine system is considered to be finished within the control volumes. This has lead to some extreme outputs during testing of the model system. Yet basing on the conclusions from literature study with considering the project scale, it has been decided that this chemical model is sufficient for answering the research questions of this project.

From the chemical model, little NO_x emission has been observed over the entire control volumes of the gas turbine system. This is contributed by the high equivalence ratio of the combustion process. With the equivalence ratio being chosen as 1.49, there are far less oxygen in the combustion chamber comparing with the fuel flow. This reductive environment has highly prevented the forming of NO_x chemicals when the system reaches the chemical balance. Over the different part-loading conditions, the NO_x emission inside the gas turbine system is limited within the level of 0.001 ppm, which is a level that far below what is worth considering.

Yet even though maintaining the very low NO_x emission in the gas turbine, for the complete COGAS system the re-heater of the HRSG may take the majority contri-

Table 4.4: Output data against different fuel injections.

Fuel injection (kg/s)	4.0	3.6	3.2	2.8	2.4	2.0	1.6
Fuel injection ratio (%)	100	90	80	70	60	50	40
Exhaust temperature (K)	842.7	857.6	879.3	915.3	969.2	1033	1120
Re-heat temperature (K)	1267	1281	1303	1339	1394	1461	1559
Molar H ₂ in exhaust (%)	6.617	6.617	6.617	6.618	6.618	6.618	6.618
NO _x emission (ppm)	9.161	10.56	12.63	18.18	25.27	35.30	39.25
NO _x emission (g/kWh)	0.065	0.079	0.102	0.167	0.291	0.569	1.477

**Figure 4.6:** NO_x emission against exhaust temperature of the gas turbine.

tribution to the total NO_x emission of the system. This has been observed in previous articles[30] for the designed point of such system. In this project, the HRSG re-heater is set as combusting the cracked hydrogen in the gas turbine exhaust at an equivalence ratio of 1.0. The level to what this process affects the NO_x under different part load conditions is analyzed with the Simulink model.

Table 4.4 lists several sets of relevant output over different fuel injection ratios. It is noticeable that with the fuel injection ratio dropping the formation of NO_x in the HRSG re-heater increases dramatically. Considering that there are little difference in the H₂ concentration in the exhaust over these loading conditions, the key reason for this increasing NO_x is the high exhaust temperature at lower fuel injections. From the fuel flow ratio of 100% to 40%, the outlet temperature of the gas turbine has been increased nearly 280K. Resulting in the re-heating temperature of the HRSG system approaching 1559K at 40% fuel injection, which is even higher than the designed TIT of the gas turbine system. With identical chemical environments, this higher temperature significantly benefits the formation of NO_x in the exhaust. Figure 4.6 gives a more direct show of the NO_x concentration over different outlet temperature of the gas turbine.

Yet despite the sharp rising of NO_x emission under these part-loading conditions, the exact concentration of NO_x in the exhaust is remained at a low level. In Table 4.4 the NO_x concentration in the exhaust with the unit ppm is translated under the unit of g/kWh, and results shows that even under the worst loading condition the NO_x production is still at the level of 1.47g/kWh, which is still below the EEDI Tier III limit of 2.0g/kWh. Considering fact that this is only calculated with the power output of the gas turbine system, the value for the full COGAS system can be even lower. However, this result is still based on the assumption of complete chemical reaction in the gas turbine, of which the kinetics still require further investigation.

4.4 SUMMARY

In this chapter, the static performance of the gas turbine model is used for analyzing the performance of the COGAS power system under both design and off-design points. A design trade-off is raised between the combustability of the exhaust in the HRSG re-heater and efficiency of the gas turbine system. It is suggested that in order to make sure the exhaust is combustable, a high equivalence ratio of 1.49 is required in the gas turbine system.

Performance of the system is then analyzed over different working conditions. It is shown that with a similar controlling method, the ammonia gas turbine system has a similar performance over part-load conditions comparing with original gas turbines. With a lower rate of cooling mass flow, the ammonia gas turbine system is able to generate more power with a lower compressor inlet flow, leading to a higher specific power of the system. A lower system efficiency is observed for the gas turbine system, but this is due to fact of additional ammonia fuel being cracked into hydrogen concentration in the exhaust. For the complete COGAS system it still has the potential of reaching high system efficiencies as the original combined cycle gas turbines do.

As for the emission, little NO_x has been observed in the gas turbine exhaust, due to the reductive chemical environment formed by the high equivalence ratio. Yet the re-heating process in the HRSG of the COGAS system still introduces NO_x emission. With the loading factor reduces, the outlet temperature of the re-heater increases due to higher exhaust temperature of the gas turbine system, leading to a higher concentration of NO_x in the final exhaust. But despite the sharp increasing under part load conditions, the NO_x emission of the designed COGAS system is still below the limit of EEDI Tier III regulation.

5

DYNAMIC BEHAVIOR AND CONSIDERATIONS OVER CONTROLLING PROCESS

With the static outputs of the model being generated and analyzed, it is able to have a further look into the dynamic mechanism of the ammonia gas turbine system being modeled. However, the higher equivalence ratio of this system has led to troubles in the controlling process of this gas turbine system. A failure has been faced when attempting to control the ammonia gas turbine system of this project.

In this chapter, the controlling method of a common gas turbine is going to be revealed, and the dynamic behaviors of the modeled gas turbine system which operates under the high equivalence ratio will be analyzed and discussed in details. With the results of this analysis, a new method for controlling the power output of gas turbines running under fuel-rich conditions is raised and briefly discussed.

5.1 FUEL CONTROL METHOD AND APPLICATION

Gas turbine is a highly non-linear system with multiple controlling parameters. Typical of these parameters include the load, shaft speed, compressor surge and stall, TIT and fuel-air ratio. Usually, these parameters can be controlled via the fuel flow rate, guide vane angle of the compressor inlet, bleed valves, etc.. In Section 4.1, a basic controlling method has been applied for keeping a constant equivalence ratio in the combustor. For the different part-load conditions, the pressure ratio, the mass flow, and the shaft speed are all changing to maintain a constant chemical environment in the combustor. Under the dynamic situation, however, this process needs to be achieved by sampling the parameters of which the data are easy to get and controlling the data that is able to change manually.

Commonly, for a multi-shaft gas turbine system applied for maritime usage, fuel injection control is still the primarily method to control the part load power delivering processes. From the static outputs in Chapter 4, it is able to observe the relationship between shaft speed, fuel flow and the output power. For each power ratio, there is a separate value of shaft speed, fuel injection ratio and several other parameters. Among these parameters the fuel injection ratio is the easiest one to be manually controlled, and the implicit functional relationship between fuel injection and the power output can be used to form a feed-forward controlling system. This is the control loop that commonly used for controlling the load of a multi shaft gas turbine. Figure 5.1 shows a typical method of using this feed-forward control. In this figure, point *a* refers to the initial condition, point *b* represents the final condition. Curve *acb* in the figure is the static loading line of the gas turbine system, with curve *amb* being the acceleration line, and the curve *bda* being the deceleration line.

From this plot, it is shown that for a common gas turbine, an acceleration process is able to be achieved by adding additional fuel flow into the system until the flow reaches its required point. Then with an opposite action there is going to observe a deceleration process. Following this method, a dynamic testing process is programmed for carrying a deceleration of the ammonia gas turbine system from a fuel injection ratio of 80% to 60%, which according to the static outputs should

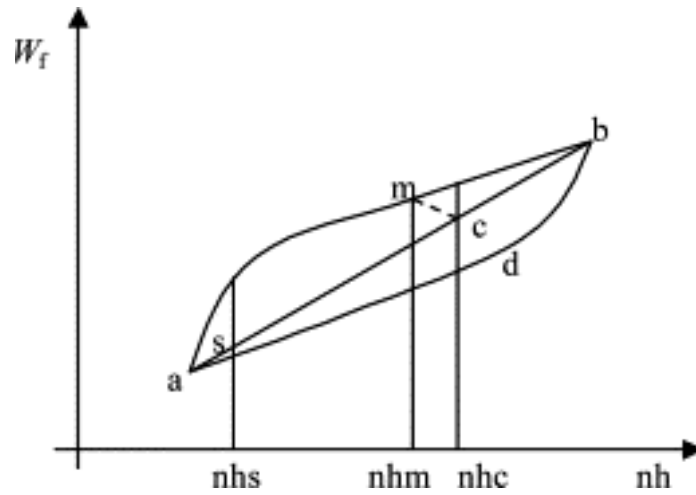


Figure 5.1: Fuel-flow rate characteristic.[51]

Table 5.1: Static data of the selected working conditions.

Fuel injection (kg/s)	3.2	2.4
Fuel injection ratio (%)	80	60
Compressor air flow (kg/s)	32.0	24.0
Compressor PR	15.473	10.891
Compressor efficiency (%)	78.50	69.96
Compressor outlet temperature (K)	748.4	714.5
Shaft speed (rpm)	8728	8208
Shaft speed ratio (%)	85.09	64.17
TIT (K)	1505	1475
High pressure turbine PR	3.368	3.535
HT efficiency (%)	83.61	76.09
HT outlet temperature (K)	1200	1192
Power turbine PR	4.594	3.081
PT efficiency (%)	85.77	79.32
Exhaust temperature (K)	879.3	969.2
Gas turbine power output (MW)	18.24	9.58
Power output ratio (%)	70.70	37.15

resulting in the power output being dropped from 70.7% to 31.75%. Typical static properties of these two loading conditions are shown in Table 5.1. In order to simplify the testing process, the fuel flow ratio is changed manually instead of applying a PID controlling system. On the other hand, several transfer function blocks are placed into the gas turbine model to prevent shock factors during its running.

However, instead of having a deceleration process as expected, the gas turbine model begins to accelerate with the lower fuel flow injection. The power output has risen from 18.24MW at the beginning to the level of 24MW when the simulation is stopped. Several dynamic results are plotted for this failed controlling process. Figure 5.2 shows the increase of compressor mass flow, Figure 5.3 shows the shaft speed, and Figure 5.4 shows the TIT temperature.

With these results it is able to conclude that the traditional fuel control method is not able to fulfill the requirement of controlling the ammonia gas turbine system which is being modelled. Before an adaptable solution could be carried out, the reason to this failure has to be located for correcting the controlling method. Basing on

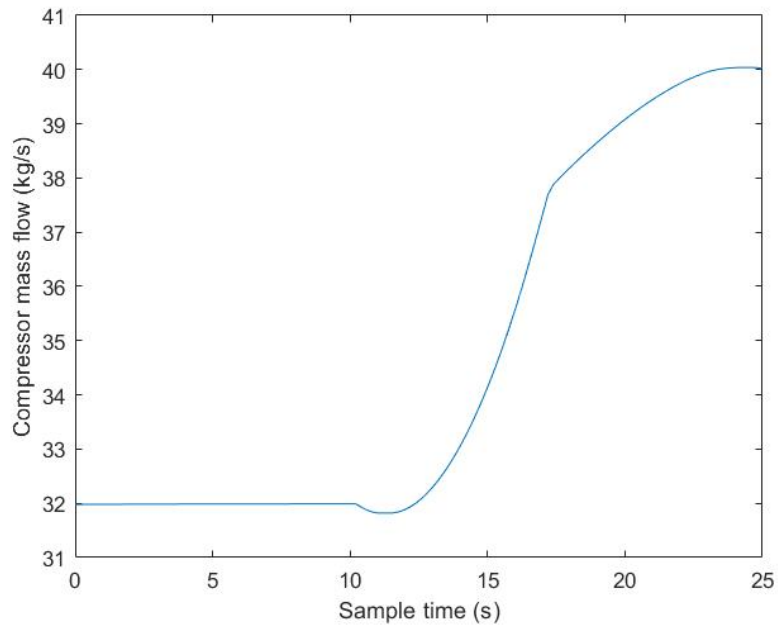


Figure 5.2: Dynamic output of the mass flow with fuel injection ratio reduced from 80% to 60%.

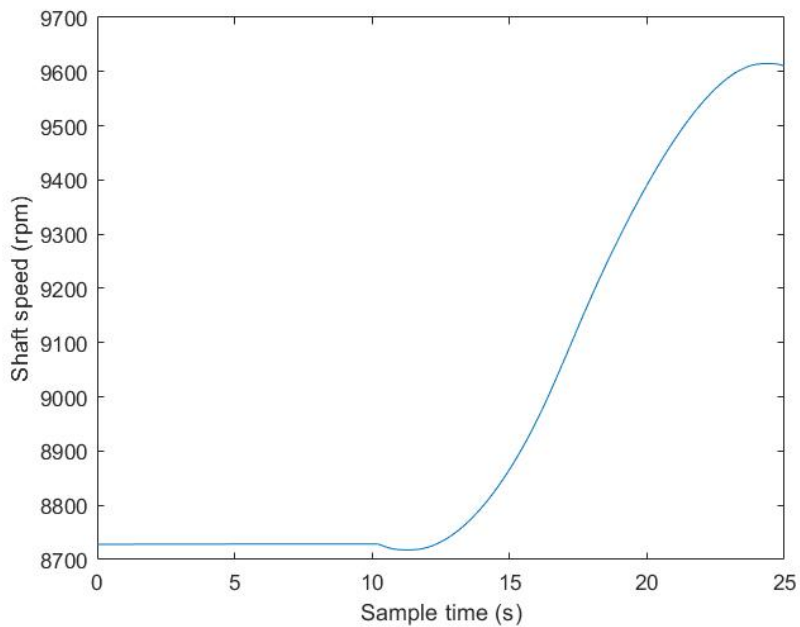


Figure 5.3: Dynamic output of shaft speed with fuel injection ratio reduced from 80% to 60%.

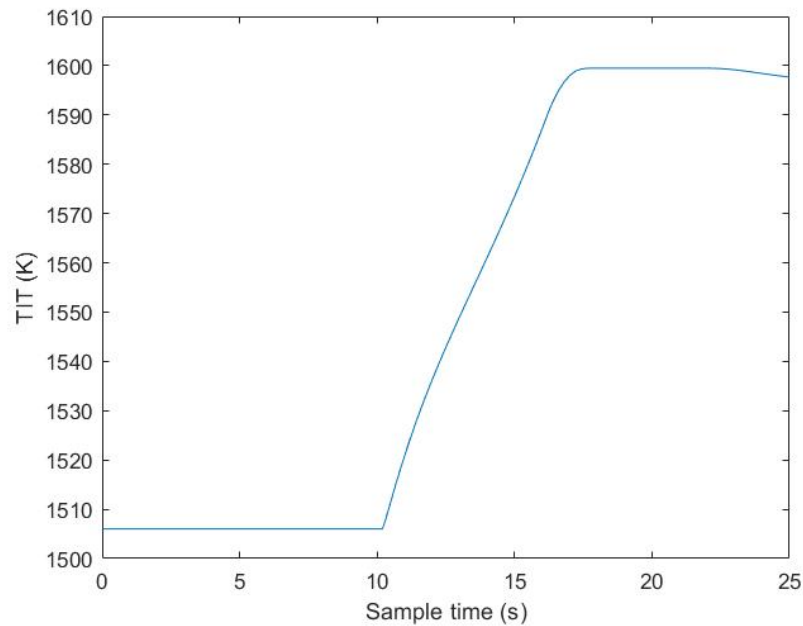


Figure 5.4: Dynamic output of the TIT with fuel injection ratio reduced from 80% to 60%.

these outputs, the reason for such performance being provided by this gas turbine model is going to be discussed in the following section.

5.2 DISCUSSING THE RESULT

In the previous section, dynamic outputs has shown that traditional fuel control method does not apply to the designed ammonia gas turbine system. New control methods have to be developed before a dynamic analysis of the system is able to be carried out. However, developing a new controlling system completely is beyond the scope and the task would be too complex for this project. Yet despite providing a complete control system, it is still able for this project to dig into the reasons of the collected dynamic behaviors of the system and analyze part of the dynamic mechanisms of this ammonia gas turbine. Basing on conclusions from these analysis, the observed dynamic behavior of the gas turbine system is able to be explained and advises can be provided for further researches.

With the gas turbine model being verified, the most probable cause of the failure would be located in the difference between the principles of this ammonia gas turbine design and traditional gas turbine systems. What probably is the most significant difference is that this ammonia gas turbine system is designed to operate under a fuel-rich condition with a very high fuel-air equivalence ratio.

In a common gas turbine which has an equivalence ratio slightly over 0.3, the combustion is taken with the amount of oxygen being far more than the amount of fuel injection. By definition, the fuel-air equivalence ratio is the current fuel-air ratio divided by the fuel-air ratio that is able to achieve a complete combustion with no additional fuel or air being left. When the fuel injection is decreased, the equivalence ratio will also decrease for both the ammonia gas turbine and the common gas turbine. For a common gas turbine system, this means the equivalence ratio is further decreased from its original value of around 0.3, hence the difference between the new equivalence ratio and the chemical equilibrium of the combustion process

becomes larger. The relationship between equivalence ratio and TIT has been shown from previous chapters in Figure 1.9. With the equivalence ratio at around 0.3, a decrease of this factor will result in a decrease of the new TIT value. This leads to a decrease of the heat flow being delivered to the next components, hence there are less heat to be converted into power via the turbine stages. So the power being delivered to both the compressor and the load will also drop, resulting in a deceleration of the gas turbine system.

However, in the ammonia gas turbine, the equivalence ratio has been set to the high value of 1.49 in order to generate a combustible amount of hydrogen from the additional fuel flow. With a slight decrease of the fuel injection similar with the common gas turbines, the fuel flow after being reduced is still above the level of a complete combustion. For the case of this project, with the reducing of fuel injection, the fuel-air equivalence ratio is reduced from 1.49 to slightly lower than 1.18. Hence to the opposite of what has happened in a common gas turbine, in the ammonia gas turbine the new combustion process becomes more close of reaching its chemical equilibrium. One factor as a result of this is the TIT begins to increase instead of the decrease in a common gas turbine, which is also the case being observed in Figure 5.4. In this case the TIT has been rising from the beginning value of 1505K to over 1600K. With little differences in the total pressure ratio and the total mass flow of the exhaust, this significant increasing of turbine inlet temperature will further increase the power being delivered by both of the driving turbine and the power turbine, resulting in a final situation that the power output and the mass flow goes through the gas turbine system being increased instead of being decreased. This is the same as what has been observed from the dynamic behaviors being shown in Figure 5.3 and Figure 5.2.

As a conclusion, the causing of the failure in applying the fuel control method to the ammonia gas turbine is due to the non-linearity located in the combustion process. This is caused by the relationship between the TIT and equivalence ratio with its range goes beyond the value of 1.0. For such fuel-rich conditions, the relationship between equivalence ratio and the TIT is just the opposite of what it is for common fuel-lean conditions. This non-linearity has broken the linear control tendency of the feed-forward controlling method being used for the fuel control solution. Although on a theoretical basis it is still able to reach the desired deceleration behavior with a non-linear tuning process of the fuel flow ratio, the complexity of such tuning process will make it not worth considering. So it would be better to introduce additional governing factors to convert this controlling process back into a linear system.

5.3 A NEW CONTROLLING SOLUTION

From the discussion in 5.2, it has been concluded that the failure in adapting the fuel control to the ammonia gas turbine system is due to the non-linearity within the control loop. From the conclusion it is considered that such problem is better to be solved by adding additional governing factors into the controlling process. By introducing an additional controlling factor that correlates to the target signal, the non-linear relationship might be able to be reduced back into a linear relationship.

In this ammonia gas turbine system, the non-linearity is located between the target of controlling turbine inlet temperature and the being controlled signal of fuel injection. These two signals are connected with the factor of the fuel-air equivalence ratio in the combustion chamber. Hence one method to linearize this system could be introducing an additional control loop to govern the equivalence ratio. From its definition, the fuel-air equivalence ratio is able to be controlled by the input signal

of fuel injection flow and the flow of oxygen from the compressor inlet. For the ammonia gas turbine system being considered in this project, the inlet flow of oxygen is able to be limited by tuning the EGR ratio, which is a signal that being able to be manually controlled in real application. This relationship is able to be figured out from 2.30. With this relationship, it could be a good idea to use the controlling of both the EGR ratio and the fuel injection flow to form a combined controlling system to limit the fuel-air equivalence ratio and hence to taking control of the power output.

5.3.1 Checking of the idea

In order to check whether this is applicable, a qualitative test is carried out on the model of this project. Due to the lack of a well designed controlling system, this test is carried out by manually tuning of the control values during a dynamic running process of the model. In order to represent the process of reducing oxygen flow together with the reducing of fuel injection, several actions are set to manually change the values that being controlled. With a starting point of 80% fuel injection, firstly the EGR ratio is increased from 0.6 to 0.7, after a few time steps the fuel injection is reduced to 60% and the EGR is tuned back to 0.65 then back to 0.6 again. This represents the behaviors that the controlling system begins to reduce the oxygen flow slightly forward than reducing the fuel injection, and as the total mass flow through the compressor begins to drop, the EGR ratio is tuned back for maintaining the required oxygen to the new fuel injection value.

Figure 5.5 shows the result of the mass flow that passes through the compressor, and the difference of the total pressure in the combustor due to such actions is shown in Figure 5.6. From the plots it is noticeable that the outlet mass flow of the compressor has been reduced from 32kg/s to the level of 24.7kg/s, and the total pressure ratio has decreased from 1547kPa to 11.77kPa. Even though this manually controlled test does not provide an accurate result, it is still managed to provide a correct tendency for the deceleration process, showing that the method of controlling both the EGR ratio and the fuel injection is an adaptable solution of controlling the power output of the ammonia gas turbine system.

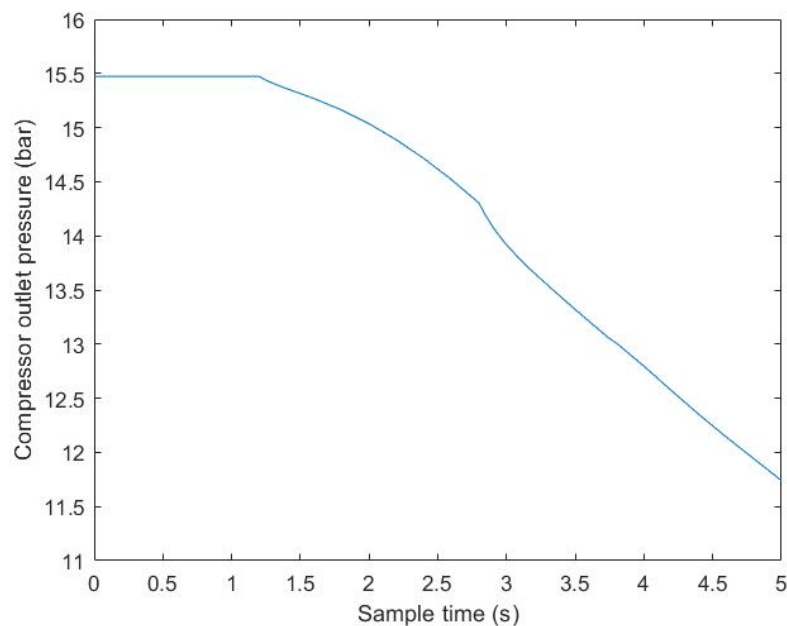


Figure 5.5: Dynamic output of the mass flow with the provided controlling process.

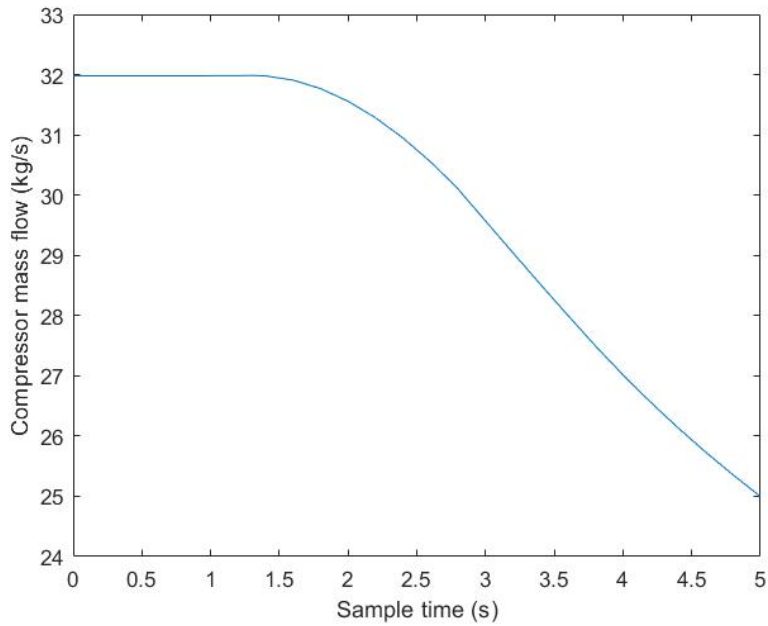


Figure 5.6: Dynamic output of the compressor outlet pressure with the provided controlling process.

5.3.2 Discussing on the new method

With the qualitative test indicating the new controlling method being adaptable, this method could be further developed into a more detailed controlling system. However, despite being able to achieve a correct outcome in behavior, there is still a non-linear tuning of the EGR ratio in the provided test. This may indicate that the new controlling process may still be a non-linear system, of which the difficulty in the tuning process may actually not much reduced. Hence a more detailed comparison is provided to compare the system complexity of the original fuel control system and the new combined fuel-EGR controlling system.

Figure 5.7 indicates the control loop of the original fuel control system. The combustor, where the non-linear behavior of the TIT locates is marked red in this diagram. It is clear that with this non-linear component the behavior of the whole gas turbine system also becomes non-linear, hence the entire system is also marked in a

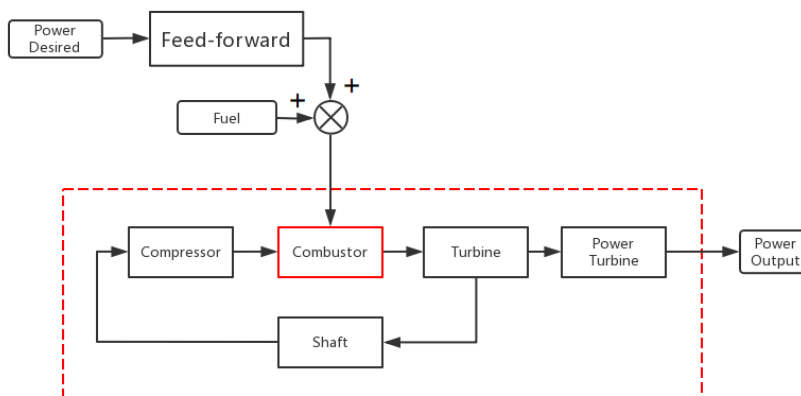


Figure 5.7: Dynamic output of the mass flow with the provided controlling process.

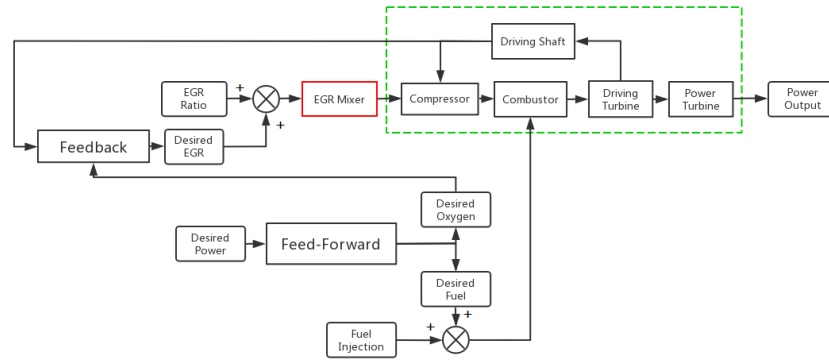


Figure 5.8: Dynamic output of the mass flow with the provided controlling process.

red block in the figure. Since the feed-forward controller needs to contain the relationship between a power requirement and the co-related variation of fuel injection ratio, the non-linearity will cause great difficulties in the designing and tuning processes.

On the other hand, in the new controlling system, by transforming the non-linearity into an additional EGR control, the rest of the system which is still under the fuel control will be able to maintain a linear behavior. This is shown in Figure 5.8, which indicates the layout of the new control system. Despite the compressor, which has been involved in the additional control loop, the rest of the gas turbine system has been marked in a green block for its linear behavior after the non-linearity has been removed.

In Figure 5.8, it is shown that the non-linearity has been red-marked and located in a separate control loop apart from the original fuel control system. This indicates the non-linear process in controlling the mass of oxygen in the inlet air flow with the feedback signal of compressor shaft speed (indicating the total mass flow through the compressor) and the disturbance of desired amount of oxygen flow. This is a feedback controlling system which only controls partial behavior of the compressor and behavior of the EGR system, which is much simpler than the original feed-forward system of the fuel control. Basing on the relationship shown in 2.22 and the static output data of the system shown in ???. It is clear that the total amount of air that passes through the compressor is able to be represented by the shaft speed of the compressor. The real oxygen flow is then able to be calculated with this total mass flow and the current EGR ratio. With such feedback signal, and together with the disturbance of the desired oxygen flow sent from the original fuel control system, a feedback controller is able to be introduced to create the desired EGR ratio with the error of oxygen flow.

Under the new controlling system, the non-linear behavior of the EGR ratio during the power switching process is able to be controlled by a linear feedback controller. This means that the new controlling method has successfully linearized the controlling process of this ammonia gas turbine system. This also indicates that the non-linear switching of the EGR ratio in the manually controlled test is not the sign of another non-linear controller, but an reaction to the behavior of the input signals. With the controlling system being linearized, the difficulty in tuning the system would be reduced significantly.

In this section, a new EGR controlling system that combines the original fuel control with an additional EGR control loop has been carried out basing on previous dis-

cussions and examined over a qualitative test. It is shown that with such a new controlling system the power output of the gas turbine is able to be controlled. The tuning process of the new system will also be simplified because both of the control loops within the new system can be carried out with linear controllers. This ensures that the new control method is able to be adapted in practical cases for controlling a gas turbine system that operations under fuel-rich conditions.

5.4 OTHER OBSERVATIONS

While analyzing the differences between the dynamic behavior of the ammonia gas turbine system and the common systems, some additional discoveries are founded in the chemical process. Figure 5.9 and Figure 5.10 shows the dynamic behavior of oxygen concentration and the NO_x emission at the outlet of the gas turbine system in the failed fuel control test. After the TIT increase due to the lower equivalence ratio, more power is delivered by the high pressure turbine to the compressor. This results in an increase of the compressor mass flow. Due to this increase of fresh air injection, the exact equivalence ratio inside the combustor was pushed beyond the line of 1.0, resulting in a slightly fuel-rich condition instead of the fuel-lean situation which the ammonia gas turbine is designed to be. This is the reason why there is a sharp increase of the oxygen concentration in the gas turbine exhaust in Figure 5.9.

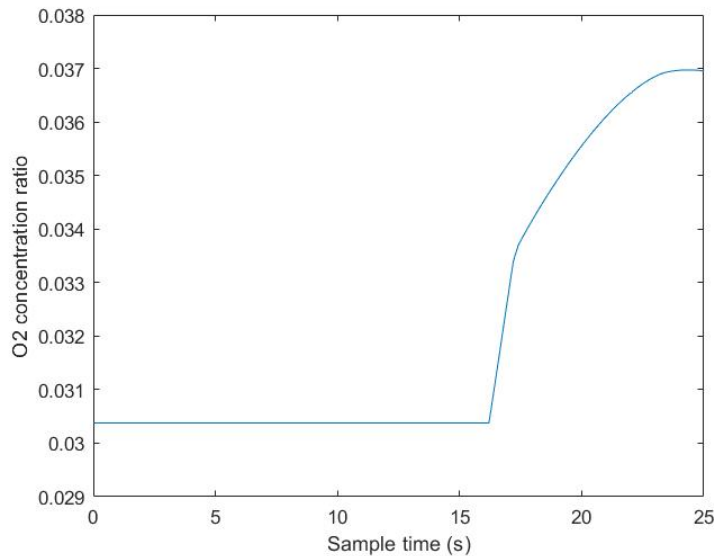


Figure 5.9: O₂ concentration output at gas turbine exhaust.

This variety of oxygen concentration provides an opportunity for a further look into the NO_x formation under different equivalence ratio and combustion environment in the gas turbine combustor. Figure 5.10 shows a sharp increase of the NO_x emission at the time step of 16s. With comparing to the result shown in Figure 5.9 it can be noticed that this is exactly the time when the equivalence ratio is pushed beyond 1.0 and additional oxygen begins to build up in the exhaust. This reveals a high sensitivity of NO_x formation to the existence of additional oxygen under the situation of chemical balance, and further reveals the importance of keeping a fuel-lean condition in the combustion process of ammonia fuel.

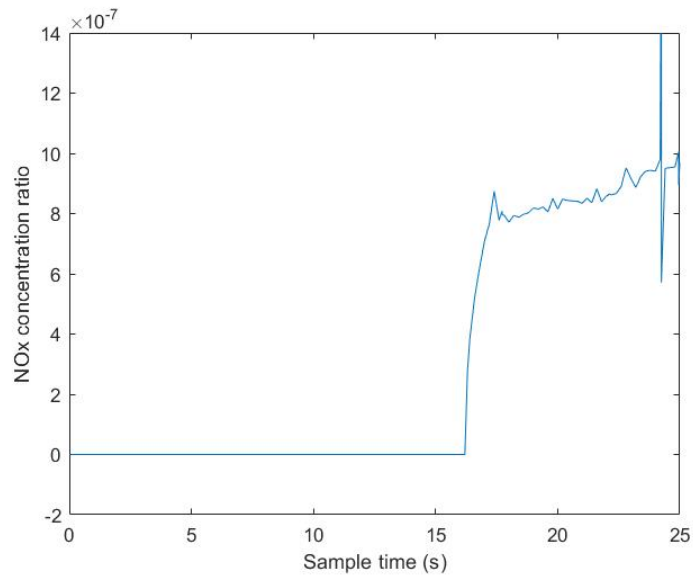


Figure 5.10: NOx concentration output at gas turbine exhaust.

5.5 SUMMARY

In this chapter, the failure of applying the fuel control method to the ammonia gas turbine system is evaluated and discussed. It is observed that with a reduction of fuel injection, the power output of the ammonia gas turbine system begins to increase instead of decrease as for a common gas turbine. The reason of this odd behavior is located at the non-linearity of the feed-forward controlling cycle of the fuel control method. Different from low equivalence ratio conditions, under a fuel lean condition the TIT is increasing when the equivalence ratio drops, resulting in more power be generated in the driving turbine which is then delivered to the compressor, hence making the situation even worse.

To solve this problem, it is suggested to have both the fuel control and the controlling of the EGR ratio being used for this ammonia gas turbine system. By controlling the EGR ratio, the non-linearity in the feed-forward fuel control loop is converted to the feedback controlling of the total oxygen inlet to the value of the EGR ratio. This largely simplifies the controlling system, and makes this method being adaptable in practical usage.

Besides, by analyzing the dynamic output of the chemical model, it is further confirmed that the existence of additional oxygen in the exhaust has a high impact on the formation of NOx emission when the mixture is approaching a chemical balance. This makes the controlling of the combustion environment of ammonia fuel even more important.

6

CONCLUSIONS AND RECOMMENDATIONS

In this project, the mechanism of the ammonia gas turbine system is further analyzed for the application of an ammonia COGAS power system on a ship based on previous researches. In the literature research phase of this project, it is concluded that future ammonia gas turbine systems will operate under a fuel-lean condition with high equivalence ratios and adapting the EGR process to control the turbine inlet temperature. Yet the performance of such a system is only on the basis of static results under a default working condition. This project is hence carried out for a further study into off-design working conditions of such a gas turbine system and evaluates the potential of having such an ammonia COGAS power system onboard ships.

Basing on the literature study, a model of the ammonia gas turbine system combining a thermal chemical solver and a dynamic mechanical solver is constructed using the Simulink tool from Matlab software to analyze the properties of such a gas turbine system under part load and dynamic working conditions. With the model being verified, several research questions are discussed basing on both the static and dynamic outputs of the Simulink model. The answers to the research questions and additional conclusions regarding some of the problems being revealed during this project is discussed in this chapter.

6.1 ANSWERS TO THE RESEARCH QUESTIONS

The main research question of this project is located on the thermal-chemical performance of an ammonia gas turbine system over dynamic loading conditions. This task has been divided into several sub-questions regarding to a variety of topics from the system performance to the formation of NO_x emission. In this section, these sub-questions are going to be answered one by one to conclude the final conclusions of this project. The questions except for the one on the modelling process are listed with their answers as below:

Sub question 1: To what level will the emissions be changed under off-design conditions?

In this project, the model is tested over different fuel injection ratios to analyze the part-load working condition of such an ammonia gas turbine. Under the assumption of complete chemical reactions, it is shown that due to the fuel-lean environment in the combustion chamber which leads to a lack of additional oxygen, the formation of NO_x emission is able to be neglected. Yet in order to deal with the hydrogen emission caused by the cracking of additional ammonia, a very high equivalence ratio has to be kept for generating a combustable concentration of H₂ in the exhaust. The combustion of hydrogen in the re-heat HRSG system can still cause formation of NO_x.

During this project, it is observed that under part loading conditions, the NO_x concentration at the HRSG outlet is increasing sharply as the load of the gas turbine drops. This is caused by the dropping of part load efficiency of the gas turbine sys-

tem, resulting in a significant increase of the exhaust temperature. The increase of NO_x emission is caused by this higher exhaust temperature which leads to a higher reheat temperature in the HRSG. Yet despite increasing sharply, the NO_x emission is still below the Tier III limitation at the lowest power put being considered in this project, which is only 7.57% of the gas turbine's designed power output. Under this situation, a NO_x emission of 1.47g/kwh is observed with only calculating the power output of the gas turbine in the COGAS power system, with the emission rate of the full system being even lower.

Sub question 2: To what level can the system be controlled to try minimizing the pollutants?

In the dynamic testing process of the model, it is shown that the traditional controlling method of the fuel control solution is not able to be adapted to this ammonia gas turbine system due to its operation under fuel-lean conditions. With the equivalence ratio being higher than 1.0, a decrease of the fuel injection will cause the TIT being raised higher, and resulting in an even higher power output of the gas turbine system. To solve this problem a controlling method of tuning both the fuel injection flow and the EGR ratio is suggested by this project. By switching the non-linearity from a complex feed-forward controlling loop into a simple feedback control, this new method largely simplifies the tuning process of the control system. In a brief test it is able to reduce both the mass flow through the compressor and the total pressure ratio of the gas turbine system when the fuel injection ratio is reduced for a deceleration of the gas turbine.

By fine tuning on the parameters of this controlling process, its disturbance to the chemical distribution of the gas turbine exhaust mixture could be minimized. With the static emission over different part loading conditions being able to fulfill the Tier III requirement, the NO_x emission during these power shifting process is also able to be limited at a low level.

Sub question 3: Which system has better performance if the ammonia COGAS is compared against an ICE system? Regarding both on system efficiency and emissions.

With the chosen parameters of the gas turbine model, it is able to deliver a power output of 25.8MW with an ammonia injection rate of 4kg/s. This results in a system efficiency of 34.68%, which is even lower than that of current gas turbine systems. However, this low efficiency is caused by the high equivalence ratio being selected for this system, which is as high as 1.49. A large amount of energy is stored in the high concentration of the formed hydrogen in the exhaust, which is still able to be recovered in the reheating HRSG system of the COGAS. It is observed that a heat flow of 60.08MJ/s can be reached at the HRSG system after combustion of this hydrogen concentration, which will result in a total efficiency of the COGAS being 54.87% with an assumed 25% efficiency of the HRSG cycle. This is comparable with the current combined cycle gas turbine systems and is significantly higher than the system efficiency of current medium-speed ICEs.

For the part loading conditions, the efficiency of the gas turbine system drops sharply due to low part load efficiency of the compressor and turbine blades. But despite this low power output in the gas turbine, the HRSG can still receive a thermal flow of 32MJ/s and an even higher inlet temperature with a 40% fuel injection. This makes the part load efficiency of this COGAS system still in an acceptable range, which basing on conclusions in the literature study will further leading to a lower operation cost in maritime usage.

With all these answers to the sub-researching questions, it is clear that the ammonia gas turbine system is able to maintain a good performance under part loading conditions, and the emission ratio is able to be remained under a low level with an improvement of its controlling method. The NO_x emission is able to be reduced under the limit of 2g/kwh from the Tier III requirement, and the part loading efficiency of the full COGAS system is still within an acceptable range. This has indicated to a bright future for the adaptation of ammonia COGAS power systems being applied on sea-going ships under an ammonia economy.

6.2 ADDITIONAL CONCLUSIONS AND RECOMMENDATIONS

Despite being able to answer the researching questions, the fact that the fuel control methods fails to match the requirements of the ammonia gas turbine has lead to a further analysis of the mechanism of gas turbine systems under high equivalence ratios. As a result of this analysis it is suggested to introduce additional controlling parameters to simplify the non-linear control loop. A method of controlling both the fuel injection and the EGR ratio is provided in this project, resulting in a correct tendency of the dynamic outputs. However, this method does not eliminate the non-linear behaviors of the signal that being controlled, hence there may still be better methods for controlling such a gas turbine system that operates under fuel-rich conditions.

Besides, the high equivalence ratio has lead to a high concentration of hydrogen in the high temperature exhaust, which can be hazardous to the material of the turbine blades. Hence a further research into dealing with corrosion and other problems that can be caused by this hydrogen concentration would be highly appreciated.

In this project, there are several assumptions being applied to simplify the modelling process. Due to technical reasons, the off-design performance of the compressor and turbine blades are approached with fitted functions. Even though the modeled compressor and turbine map models of this project has been verified, there is still a lack of validation to the model due to lack of practical examples. This may cause troubles that the modeled map blocks may not able to accurately reflect the behaviors of real turbine systems. A better approximation of the turbine behavior would improve the accuracy of further simulation analysis.

Among the assumptions being applied in this project, the most significant one is that the chemical model of this project is constructed basing on the assumption of a complete chemical reaction. It is assumed that the chemical mixture is able to reach a stable condition within each control volume of the model systems, which is based on kinetic analysis and other previous literature references, and not fully corresponding to the experiment results from micro-turbine systems[11][16][31][43]. What may exactly happen to the chemical kinetics and how will the difference influence the NO_x emission of such COGAS system under the relatively high pressure ratios and temperature ratios of a maritime gas turbine will be of highly interested for further analysis.

All in all, this project provides a further review over the adaptation of the ammonia COGAS power system on a maritime sight of view. Analysis on basic properties of the fuel-lean operated ammonia gas turbine system is taken to the level of part loading conditions with a slight level of dynamic behaviors. A new method for controlling such a system is raised and a brief verification is provided for its adaptability. Suggestions on further researches over this project is provided basing on

the problems and limits being faced during the analyzing processes. Hopefully this will be beneficial to the construction of a cleaner maritime world in the near future.

BIBLIOGRAPHY

- [1] IMO, *Imo action to reduce greenhouse gas emissions from international shipping*. [Online]. Available: <https://wwwcdn.imo.org/localresources/en/MediaCentre/HotTopics/Documents/>.
- [2] M. B.-H. et al., "Carbon capture and storage update", *Energy Environmental Science*, vol. 7, pp. 130–189, 2014. DOI: <https://doi.org/10.1039/c3ee42350f>.
- [3] J. Witcover and R. B. Williams, "Comparison of "advanced" biofuel cost estimates: Trends during rollout of low carbon fuel policies", *Transportation Research Part D: Transport and Environment*, vol. 79, pp. 102–211, 2020. DOI: <https://doi.org/10.1016/j.trd.2019.102211>.
- [4] Engineering Toolbox. (). "Boiling points for common liquids and gases", [Online]. Available: https://www.engineeringtoolbox.com/boiling-points-fluids-gases-d_155.html.
- [5] A. Dana, O. Elishav, A. Bardow, G. E. Shter, and G. S. Grader, "Nitrogen-based fuels: A power-to-fuel-to-power analysis", *Angewandte Chemie International Edition*, vol. 55, pp. 8798–8805, 2016. DOI: <https://doi.org/10.1002/anie.201510618>.
- [6] J. D. James and Y. C. van Delft, "Power to ammonia process options: Input to power to ammonia value chains and business cases", 2017. [Online]. Available: <https://publicaties.ecn.nl/PdfFetch.aspx?nr=ECN-E--17-039>.
- [7] C. Lhuillier, P. Brequigny, F. Contino, and C. Mounaïm-Rousselle, "Experimental study on ammonia/hydrogen/air combustion in spark ignition engine conditions", *Fuel*, vol. 269, pp. 117–448, 2020. DOI: <https://doi.org/10.1016/j.fuel.2020.117448>.
- [8] B. T. W. Mestemaker, M. B. G. Castro, E. C. van der Blom, H. J. Cornege, and K. Visser, "Zero emission vessels from a shipbuilders perspective", Glasgow, United Kingdom, 2019. [Online]. Available: https://www.researchgate.net/publication/334480164_Zero_emission_vessels_from_a_shipbuilders_perspective.
- [9] National Institute of Standard and Technology. (). "Nist chemistry webbook", [Online]. Available: <https://webbook.nist.gov/>.
- [10] A. A. Wright and T. S. Wilson, "Flashpoint of marine distillate oil fuels: Issues and implications associated with the harmonization of the minimum flashpoint requirement for marine distillate oil fuels with that of other users", 2012. [Online]. Available: <https://wwwcdn.imo.org/localresources/en/MediaCentre/HotTopics/Documents/>.
- [11] J. Otomo, M. Koshi, T. Mitsumori, H. Iwasaki, and K. Yamada, "Chemical kinetic modeling of ammonia oxidation with improved reaction mechanism for ammonia/air and ammonia/hydrogen/air combustion", *International Journal of Hydrogen Energy*, vol. 43, pp. 3004–3014, 2018. DOI: <https://doi.org/10.1016/j.ijhydene.2017.12.066>.
- [12] A. Reiter and S. Kong, "Demonstration of compression-ignition engine combustion using ammonia in reducing greenhouse gas emissions", *Energy Fuels*, vol. 22, pp. 2693–2971, 2008. DOI: <https://doi.org/10.1021/ef800140f>.
- [13] K. Ryu, G. E. Zacharakis-Jutz, and S. Kong, "Effects of gaseous ammonia direct injection on performance characteristics of a spark-ignition engine", *Applied Energy*, vol. 116, pp. 206–215, 2014. DOI: <https://doi.org/10.1016/j.apenergy.2013.11.067>.

- [14] A. Medina, J. M. M. Roco, and A. C. Hernández, "Regenerative gas turbines at maximum power density conditions", *Journal of Physics D: Applied Physics*, vol. 29, pp. 2802–2805, 1997. DOI: [10.1088/0022-3727/29/11/011](https://doi.org/10.1088/0022-3727/29/11/011).
- [15] H. S. et al., "Integration of solid oxide fuel cell and internal combustion engine for maritime applications", *Applied Energy*, vol. 281, p. 115 854, 2021. DOI: <https://doi.org/10.1016/j.apenergy.2020.115854>.
- [16] E. C. Okafor, K. Kunkuma, A. Somarathne, A. Hayakawa, T. Kudo, O. Kurata, N. Iki, and H. Kobayashi, "Towards the development of an efficient low-nox ammonia combustor for a micro gas turbine", *Proceedings of the Combustion Institute*, vol. 37, pp. 4597–4606, 2019. DOI: <https://doi.org/10.1016/j.proci.2018.07.083>.
- [17] GE Aviation, *Lm2500 marine gas turbine*. [Online]. Available: <https://www.geaviation.com/marine/engines/military/lm2500-engine>.
- [18] MAN Diesel, *Marine engine programme 3rd edition 2006: V32/44cr*, 2006. [Online]. Available: <https://www.geaviation.com/marine/engines/military/lm2500-engine>.
- [19] G. Benvenuto, M. Laviola, and U. Campora, "Assessment of steam cycle layouts for cogas ship propulsion systems", 2015. DOI: <https://doi.org/10.1201/b17494-99>.
- [20] M. Atmaca, "Efficiency analysis of combined cogeneration systems with steam and gas turbines", *Energy Sources, Part A: Recovery, Utilization and Environmental Effects Part A: Recovery*, vol. 4, pp. 360–369, 2011. DOI: <https://doi.org/10.1080/15567031003741434>.
- [21] GE Power, "Gas power systems offerings", 2019. [Online]. Available: https://www.ge.com/content/dam/gepower-pgdp/global/en_US/documents/product/gas-power-systems-product-catalog-2019.pdf.
- [22] D. McLarty, J. Brouwer, and S. Samuelsen, "Fuel cell-gas turbine hybrid system design part ii: Dynamics and control", *Journal of Power Sources*, vol. 254, pp. 126–136, 2014. DOI: <https://doi.org/10.1016/j.jpowsour.2013.11.123>.
- [23] Automotive world. (2020). "Bosch and weichai power increase efficiency of weichai truck diesel engines to 50 percent", [Online]. Available: <https://www.automotiveworld.com/news-releases/>.
- [24] GTT, CMA-CGM, and DNV-GL, "Lng fuelled perfect piston engine room free efficient containership", 2015. [Online]. Available: <https://www.dnv.com/Images/>.
- [25] F. Haglind, "A review on the use of gas and steam turbine combined cycles as prime movers for large ships. part ii: Previous work and implications", *Energy Conversion and Management*, vol. 49, pp. 3468–3475, 2008. DOI: <https://doi.org/10.1016/j.enconman.2008.08.004>.
- [26] I. Ahlqvist, *Electric Propulsion : The Effective Solution Conference Proceedings*. London: Institute of Marine Engineers, 1995, ISBN: 978-0907206651.
- [27] SBIR. (2013). "Ultra-high power density solid oxide fuel cell stack for high efficiency propulsion and power systems", [Online]. Available: <https://www.sbir.gov/node/413464>.
- [28] D. U. et al., "Metal-supported solid oxide fuel cells with exceptionally high power density for range extender systems", *Cell Reports Physical Science*, vol. 1, p. 100 072, 2020. DOI: <https://doi.org/10.1016/j.xcrp.2020.100072>.
- [29] Battelle Memorial Institute, "Manufacturing cost analysis of 100 and 250 kw fuel cell systems for primary power and combined heat and power applications", 2016. [Online]. Available: https://www.energy.gov/sites/prod/files/2016/07/f33/fcto_battelle_mfg_cost_analysis_pp_chp_fc_systems.pdf.

- [30] V. Mrzljak and T. Mrakovčić, “Comparison of coges and diesel-electric ship propulsion systems”, *Journal of Maritime Transportation Science*, vol. Sp. 1, pp. 131–148, 2016. DOI: <https://doi.org/10.18048/2016-00.131>.
- [31] M. Keller, M. Koshi, J. Otomo, H. Iwasaki, T. Mitsumori, and K. Yamada, “Thermodynamic evaluation of an ammonia-fueled combined-cycle gas turbine process operated under fuel-rich conditions”, *Energy*, vol. 194, p. 116 894, 2020. DOI: <https://doi.org/10.1016/j.energy.2020.116894>.
- [32] S. E. Veyo, S. D. Vora, K. P. Litzinger, and W. L. Lundberg, “Status of pressurized sofc/gas turbine power system development at siemens westinghouse”, 2002. DOI: <https://doi.org/10.1115/GT2002-30670>.
- [33] K. Miyamoto, M. Mihara, H. Oozawa, K. Hiwatashi, K. Tomida, M. Nishiura, H. Kishizawa, R. Mori, and Y. Kobayashi, “Recent progress of sofc combined cycle system with segmented-in-series tubular type cell stack at mhps”, *ECS Transactions*, vol. 68, pp. 51–58, 2015. DOI: <https://doi.org/10.1149/06801.0051ecst>.
- [34] M. Metcalfe, S. Burke, S. Ahmed, and H. Curran, “A hierarchical and comparative kinetic modeling study of c1 c2 hydrocarbon and oxygenated fuels”, *International Journal of Chemical Kinetics*, vol. 45, 2013. DOI: <https://doi.org/10.1002/kin.20802>.
- [35] Y. Song, H. Hashemi, J. M. Christensen, P. M. C. Zou, and P. Glarborg, “Ammonia oxidation at high pressure and intermediate temperatures”, *Fuel*, vol. 181, pp. 358–365, 2016. DOI: <https://doi.org/10.1016/j.fuel.2016.04.100>.
- [36] E. Hu, H. Li, X. Meng, Y. Chen, T. Cheng, Y. Xie, and Z. Huang, “Laminar flame speeds and ignition delay times of methane–air mixtures at elevated temperatures and pressures”, *Fuel*, vol. 158, pp. 1–10, 2015. DOI: <https://doi.org/10.1016/j.fuel.2015.05.010>.
- [37] A. Valera-Medina, H. Xiao, M. Owen-Jones, W. I. F. David, and P. J. Bowen, “Ammonia for power”, *Progress in Energy and Combustion Science*, vol. 69, pp. 63–102, 2018. DOI: <https://doi.org/10.1016/j.pecs.2018.07.001>.
- [38] *MARPOL Regulations for the Prevention of Air Pollution from Ships, Regulation 13 - Nitrogen oxides (NOx)*, 2008. [Online]. Available: [https://www.imo.org/en/OurWork/Environment/Pages/Nitrogen-oxides-\(NOx\)%E2%80%93Regulation-13.aspx](https://www.imo.org/en/OurWork/Environment/Pages/Nitrogen-oxides-(NOx)%E2%80%93Regulation-13.aspx).
- [39] H. J. K. Woud and D. Stapersma, *Design of Propulsion and Electric Power Generations Systems*. London: IMarEST, The Institute of Marine Engineering, Science and Technology, 2002, ISBN: 1-902536-47-9.
- [40] Foundation for Change. (2020). “Systems thinking handout”, [Online]. Available: <https://www.foundationforchange.org.uk/systems-thinking-handout>.
- [41] FAS military analysis network. (1999). “Lm2500 gas turbine engine”, [Online]. Available: <https://fas.org/man/dod-101/sys/ship/eng/lm2500.htm>.
- [42] *GPSA Engineering Data Book*, 13th ed. Calgary: Gas Processing Association Canada, 2012, ISBN: 978-9998095533.
- [43] Y. Ying, Y. Cao, S. Li, and Z. Wang, “Study on flow parameters optimisation for marine gas turbine intercooler system based on simulation experiment”, *Int. J. Computer Applications in Technology*, vol. 47, pp. 57–67, 2013. DOI: <https://doi.org/10.1504/IJCAT.2013.054302>.
- [44] M. Lanchi, M. Montecchi, T. Crescenzi, D. Mele, A. Miliozzi, V. Russa, D. Mazzei, M. Misceo, M. Falchetta, and R. Mancini, “Investigation into the coupling of micro gas turbines with csp technology: Omsop project”, *Energy Procedia*, vol. 69, pp. 1317–1326, 2015. DOI: <https://doi.org/10.1016/j.egypro.2015.03.146>.

- [45] *Mark's Standard Handbook for Mechanical Engineers*, 7th ed. New York: McGraw Hill Book Co., 1967, ISBN: 9781112412844.
- [46] E. Tsoutsanis, Y. G. Li, P. Pilidis, and M. Newby, "Part-load performance of gas turbines – part i: A novel compressor map generation approach suitable for adaptive simulation", 2012. DOI: <https://doi.org/10.1115/GTINDIA2012-9580>.
- [47] A. Maria, "Introduction to modelling and simulation", 1997.
- [48] P. Colonna and H. van Putten, "Dynamic modeling of steam power cycles.: Part i—modeling paradigm and validation", *Applied Thermal Engineering*, vol. 27, pp. 467–480, 2007. DOI: <https://doi.org/10.1016/j.applthermaleng.2006.06.011>.
- [49] A. Vrijdag, "Control of propeller cavitation in operational conditions", 2009.
- [50] *Guideline for Use of Hydrogen and Flammable Hydrogen Gas Mixtures*, 2011. [Online]. Available: <https://engineering.purdue.edu/ChE/aboutus/safety/documents/hydrogen-use-guidelines-october-2011.pdf>.
- [51] Y. Yu, L. Chen, F. Sun, and C. Wu., "Matlab/simulink-based simulation for digital-control system of marine three-shaft gas-turbine", *Applied Energy*, vol. 80, pp. 1–10, 2005. DOI: <https://doi.org/10.1016/j.apenergy.2004.03.006>.

APPENDICES

A

MATLAB CODE FOR CHEMICAL MODEL

The following two sets of Matlab codes shows how the chemical solver is referenced by the main Simulink model and how it is built up. The reference code is implemented in the fcn block in the Simulink model, and the solver is coded in a separated Matlab file. This method avoids the limitation that Simulink cannot solve a double-loop function system, and solves the chemical solver with the more powerful Matlab system.

There are four chemical solvers applied in the Simulink model, the combustor, the driving turbine, the power turbine and the HRSG re-heater. Hence four sets of this Matlab code are attached to fulfill the requirement of these sub systems. This appendix applies the code set used in the chemical solver of the combustor.

The referencing coder applied in the fcn block of the Simulink model:

```
function [y1, y2] = chemicalbalance(To, beq, xo, P)
% Declare function name in the fcn block
coder.extrinsic('opt_chemical');
% Informing the Coder
y1 = [0,0,0,0,0,0,0,0,0,0,0,0,0];
% Initial value, to receive the chemical concentration data from the main solver
y2 = 0;
% Initial value, to receive the final temperature data from the main solver
disp(y1);
% For checking the output data in the message window
[y1, y2] = opt_chemical(To, beq, xo, P);
% Connecting the main solver file, sending the inputs and receiving the outputs
end
```

The referenced Matlab code:

```

function [y1,y2] = opt_chemical(To,beq,xo,P)
% Find matching temperature for the thermal balance
global x1
% Declare global for using in both functions
To = To;
% Get input temperautre
beq = beq;
% Get element distribution
xo = xo;
% Get chemical distribution as initiate value
P = P/101325;
% Pa to bar
option1 = optimset('Algorithm','sqp');
% Option for fzero
to = To/1000;
% Input temperature for NIST calculation
t = fzero(@chebalance,to,option1);
% Get chemical distribution from fmincon function
% fzero solver for generate the enthalpy balance point
y1 = x1/sum(x1);
% Outputs chemical distribution
y2 = 1000*t;
% Outputs temperature in Kelvin

function Hbalance = chebalance(t)
% Minimizing system Gibbs free energy
t=max(t,1e-6);
t=min(t,3);
% Preventing minus value
T = 1000*t;
% The var in this function is "t", so T=1000t to generate the temperature
for each loop
to = To/1000;
% Input temperature for NIST calculation
R = 8.314e-3;
% kJ/mol/K
Po = 1;
% atm, this is the standard state pressure
T.H = [t; t.^2./2; t.^3./3; t.^4./4; -1./t; 1; 0; 0];
% For calculating Htot. Hf_298 has been added with the H factor being 0
T.Ho = [to; to^2/2; to^3/3; to^4/4; -1/to; 1; 0; 0];
% For calculating input ref enthalpy (Htoto).
Hf_298 has been added with the H factor being 0
T.S = [log(t); t; t^2/2; t^3/3; -1/(2*t^2); 0; 1; 0];
% For calculating entropy.
% NIST database list
WBo = [28.98641 1.853978 -9.647459 16.63537 0.000117 -8.671914
226.4168 0.0 % N2
31.32234 -20.23531 57.86644 -36.50624 -0.007374 -8.903471
246.7945 0.0 % O2
20.78600 2.825911e-7 -1.464191e-7 1.092131e-8 -3.661371e-8 -6.197350
179.9990 0.0 % Ar
33.066178 -11.363417 11.432816 -2.772874 -0.158558 -9.980797
172.707974 0.0 % H2
30.09200 6.832514 6.793435 -2.534480 0.082139 -250.8810
223.3967 -241.8264 % H2O
34.25667 55.18445 -35.15443 9.087440 -0.422157 -149.9098
257.0604 -136.1064 % H2O2
20.78603 4.850638e-10 -1.582916e-10 1.525102e-11 3.196347e-11 211.8020
139.8711 217.9994 % H
26.00960 34.85810 -16.30060 3.110441 -0.018611 -7.140991
250.7660 2.092001 % HO2
19.99563 49.77119 -15.37599 1.921168 0.189174 -53.30667
203.8591 -45.89806 % NH3
27.67988 51.14898 -30.64454 6.847911 -0.157906 71.24934
238.6164 82.04824 % N2O
23.83491 12.58878 -1.139011 -1.497459 0.214194 83.35783
237.1219 90.29114 % NO
16.10857 75.89525 -54.38740 14.30777 0.239423 26.17464
240.5386 33.09502 % NO2
32.27768 -11.36291 13.60545 -3.846486 -0.001335 29.75113
225.5783 38.98706]; % OH

```

```

if T<=500
% N2 data change

WB = [28.98641 1.853978 -9.647459 16.63537 0.000117 -8.671914
226.4168 0.0 % N2
31.32234 -20.23531 57.86644 -36.50624 -0.007374 -8.903471
246.7945 0.0 % O2
20.78600 2.825911e-7 -1.464191e-7 1.092131e-8 -3.661371e-8 -6.197350
179.9990 0.0 % Ar
33.066178 -11.363417 11.432816 -2.772874 -0.158558 -9.980797
172.707974 0.0 % H2
30.09200 6.832514 6.793435 -2.534480 0.082139 -250.8810
223.3967 -241.8264 % H2O
34.25667 55.18445 -35.15443 9.087440 -0.422157 -149.9098
257.0604 -136.1064 % H2O2
20.78603 4.850638e-10 -1.582916e-10 1.525102e-11 3.196347e-11 211.8020
139.8711 217.9994 % H
26.00960 34.85810 -16.30060 3.110441 -0.018611 -7.140991
250.7660 2.092001 % HO2
19.99563 49.77119 -15.37599 1.921168 0.189174 -53.30667
203.8591 -45.89806 % NH3
27.67988 51.14898 -30.64454 6.847911 -0.157906 71.24934
238.6164 82.04824 % N2O
23.83491 12.58878 -1.139011 -1.497459 0.214194 83.35783
237.1219 90.29114 % NO
16.10857 75.89525 -54.38740 14.30777 0.239423 26.17464
240.5386 33.09502 % NO2
32.27768 -11.36291 13.60545 -3.846486 -0.001335 29.75113
225.5783 38.98706]; % OH

elseif T<=700
% O2 data change

WB = [19.50583 19.88705 -8.598535 1.369784 0.527601 -4.935202
212.3900 0.0 % N2
31.32234 -20.23531 57.86644 -36.50624 -0.007374 -8.903471
246.7945 0.0 % O2
20.78600 2.825911e-7 -1.464191e-7 1.092131e-8 -3.661371e-8 -6.197350
179.9990 0.0 % Ar
33.066178 -11.363417 11.432816 -2.772874 -0.158558 -9.980797
172.707974 0.0 % H2
30.09200 6.832514 6.793435 -2.534480 0.082139 -250.8810
223.3967 -241.8264 % H2O
34.25667 55.18445 -35.15443 9.087440 -0.422157 -149.9098
257.0604 -136.1064 % H2O2
20.78603 4.850638e-10 -1.582916e-10 1.525102e-11 3.196347e-11 211.8020
139.8711 217.9994 % H
26.00960 34.85810 -16.30060 3.110441 -0.018611 -7.140991
250.7660 2.092001 % HO2
19.99563 49.77119 -15.37599 1.921168 0.189174 -53.30667
203.8591 -45.89806 % NH3
27.67988 51.14898 -30.64454 6.847911 -0.157906 71.24934
238.6164 82.04824 % N2O
23.83491 12.58878 -1.139011 -1.497459 0.214194 83.35783
237.1219 90.29114 % NO
16.10857 75.89525 -54.38740 14.30777 0.239423 26.17464
240.5386 33.09502 % NO2
32.27768 -11.36291 13.60545 -3.846486 -0.001335 29.75113
225.5783 38.98706]; % OH

```

```
elseif T<=1000
% H2 data change
```

```
WB = [19.50583 19.88705 -8.598535 1.369784 0.527601 -4.935202
212.3900 0.0 % N2
30.03235 8.772972 -3.988133 0.788313 -0.741599 -11.32468
236.1663 0.0 % O2
20.78600 2.825911e-7 -1.464191e-7 1.092131e-8 -3.661371e-8 -6.197350
179.9990 0.0 % Ar
33.066178 -11.363417 11.432816 -2.772874 -0.158558 -9.980797
172.707974 0.0 % H2
30.09200 6.832514 6.793435 -2.534480 0.082139 -250.8810
223.3967 -241.8264 % H2O
34.25667 55.18445 -35.15443 9.087440 -0.422157 -149.9098
257.0604 -136.1064 % H2O2
20.78603 4.850638e-10 -1.582916e-10 1.525102e-11 3.196347e-11 211.8020
139.8711 217.9994 % H
26.00960 34.85810 -16.30060 3.110441 -0.018611 -7.140991
250.7660 2.092001 % HO2
19.99563 49.77119 -15.37599 1.921168 0.189174 -53.30667
203.8591 -45.89806 % NH3
27.67988 51.14898 -30.64454 6.847911 -0.157906 71.24934
238.6164 82.04824 % N2O
23.83491 12.58878 -1.139011 -1.497459 0.214194 83.35783
237.1219 90.29114 % NO
16.10857 75.89525 -54.38740 14.30777 0.239423 26.17464
240.5386 33.09502 % NO2
32.27768 -11.36291 13.60545 -3.846486 -0.001335 29.75113
225.5783 38.98706]; % OH
```

```
elseif T<=1200
% NO & NO2 data change
```

```
WB = [19.50583 19.88705 -8.598535 1.369784 0.527601 -4.935202
212.3900 0.0 % N2
30.03235 8.772972 -3.988133 0.788313 -0.741599 -11.32468
236.1663 0.0 % O2
20.78600 2.825911e-7 -1.464191e-7 1.092131e-8 -3.661371e-8 -6.197350
179.9990 0.0 % Ar
18.563083 12.257357 -2.859786 0.268238 1.977990 -1.147438
156.288133 0.0 % H2
30.09200 6.832514 6.793435 -2.534480 0.082139 -250.8810
223.3967 -241.8264 % H2O
34.25667 55.18445 -35.15443 9.087440 -0.422157 -149.9098
257.0604 -136.1064 % H2O2
20.78603 4.850638e-10 -1.582916e-10 1.525102e-11 3.196347e-11 211.8020
139.8711 217.9994 % H
26.00960 34.85810 -16.30060 3.110441 -0.018611 -7.140991
250.7660 2.092001 % HO2
19.99563 49.77119 -15.37599 1.921168 0.189174 -53.30667
203.8591 -45.89806 % NH3
27.67988 51.14898 -30.64454 6.847911 -0.157906 71.24934
238.6164 82.04824 % N2O
23.83491 12.58878 -1.139011 -1.497459 0.214194 83.35783
237.1219 90.29114 % NO
16.10857 75.89525 -54.38740 14.30777 0.239423 26.17464
240.5386 33.09502 % NO2
32.27768 -11.36291 13.60545 -3.846486 -0.001335 29.75113
225.5783 38.98706]; % OH
```

```

elseif T<=1300
% OH data change

    WB = [19.50583 19.88705 -8.598535 1.369784 0.527601 -4.935202
212.3900 0.0 % N2
        30.03235 8.772972 -3.988133 0.788313 -0.741599 -11.32468
236.1663 0.0 % O2
        20.78600 2.825911e-7 -1.464191e-7 1.092131e-8 -3.661371e-8 -6.197350
179.9990 0.0 % Ar
        18.563083 12.257357 -2.859786 0.268238 1.977990 -1.147438
156.288133 0.0 % H2
        30.09200 6.832514 6.793435 -2.534480 0.082139 -250.8810
223.3967 -241.8264 % H2O
        34.25667 55.18445 -35.15443 9.087440 -0.422157 -149.9098
257.0604 -136.1064 % H2O2
        20.78603 4.850638e-10 -1.582916e-10 1.525102e-11 3.196347e-11 211.8020
139.8711 217.9994 % H
        26.00960 34.85810 -16.30060 3.110441 -0.018611 -7.140991
250.7660 2.092001 % HO2
        19.99563 49.77119 -15.37599 1.921168 0.189174 -53.30667
203.8591 -45.89806 % NH3
        27.67988 51.14898 -30.64454 6.847911 -0.157906 71.24934
238.6164 82.04824 % N2O
        35.99169 0.957170 -0.148032 0.009974 -3.004088 73.10787
246.1619 90.29114 % NO
        56.82541 0.738053 -0.144721 0.009777 -5.459911 2.846456
290.5056 33.09502 % NO2
        32.27768 -11.36291 13.60545 -3.846486 -0.001335 29.75113
225.5783 38.98706]; % OH

elseif T<=1400
% N2O & NH3 data change

    WB = [19.50583 19.88705 -8.598535 1.369784 0.527601 -4.935202
212.3900 0.0 % N2
        30.03235 8.772972 -3.988133 0.788313 -0.741599 -11.32468
236.1663 0.0 % O2
        20.78600 2.825911e-7 -1.464191e-7 1.092131e-8 -3.661371e-8 -6.197350
179.9990 0.0 % Ar
        18.563083 12.257357 -2.859786 0.268238 1.977990 -1.147438
156.288133 0.0 % H2
        30.09200 6.832514 6.793435 -2.534480 0.082139 -250.8810
223.3967 -241.8264 % H2O
        34.25667 55.18445 -35.15443 9.087440 -0.422157 -149.9098
257.0604 -136.1064 % H2O2
        20.78603 4.850638e-10 -1.582916e-10 1.525102e-11 3.196347e-11 211.8020
139.8711 217.9994 % H
        26.00960 34.85810 -16.30060 3.110441 -0.018611 -7.140991
250.7660 2.092001 % HO2
        19.99563 49.77119 -15.37599 1.921168 0.189174 -53.30667
203.8591 -45.89806 % NH3
        27.67988 51.14898 -30.64454 6.847911 -0.157906 71.24934
238.6164 82.04824 % N2O
        35.99169 0.957170 -0.148032 0.009974 -3.004088 73.10787
246.1619 90.29114 % NO
        56.82541 0.738053 -0.144721 0.009777 -5.459911 2.846456
290.5056 33.09502 % NO2
        28.74701 4.714489 -0.814725 0.054748 -2.747829 26.41439
214.1166 38.98706]; % OH

```

```

elseif T<=1700
% H2O data change

    WB = [19.50583 19.88705 -8.598535 1.369784 0.527601 -4.935202
212.3900 0.0 % N2
        30.03235 8.772972 -3.988133 0.788313 -0.741599 -11.32468
236.1663 0.0 % O2
        20.78600 2.825911e-7 -1.464191e-7 1.092131e-8 -3.661371e-8 -6.197350
179.9990 0.0 % Ar
        18.563083 12.257357 -2.859786 0.268238 1.977990 -1.147438
156.288133 0.0 % H2
        30.09200 6.832514 6.793435 -2.534480 0.082139 -250.8810
223.3967 -241.8264 % H2O
        34.25667 55.18445 -35.15443 9.087440 -0.422157 -149.9098
257.0604 -136.1064 % H2O2
        20.78603 4.850638e-10 -1.582916e-10 1.525102e-11 3.196347e-11 211.8020
139.8711 217.9994 % H
        26.00960 34.85810 -16.30060 3.110441 -0.018611 -7.140991
250.7660 2.092001 % HO2
        52.02427 18.48801 -3.765128 0.248541 -12.45799 -85.53895
223.8022 -45.89806 % NH3
        60.30274 1.034566 -0.192997 0.012540 -6.860254 48.61390
272.5002 82.04824 % N2O
        35.99169 0.957170 -0.148032 0.009974 -3.004088 73.10787
246.1619 90.29114 % NO
        56.82541 0.738053 -0.144721 0.009777 -5.459911 2.846456
290.5056 33.09502 % NO2
        28.74701 4.714489 -0.814725 0.054748 -2.747829 26.41439
214.1166 38.98706]; % OH

elseif T<=2000
% N2 & O2 & HO2 data change

    WB = [19.50583 19.88705 -8.598535 1.369784 0.527601 -4.935202
212.3900 0.0 % N2
        30.03235 8.772972 -3.988133 0.788313 -0.741599 -11.32468
236.1663 0.0 % O2
        20.78600 2.825911e-7 -1.464191e-7 1.092131e-8 -3.661371e-8
-6.197350 179.9990 0.0 % Ar
        18.563083 12.257357 -2.859786 0.268238 1.977990 -1.147438
156.288133 0.0 % H2
        41.96426 8.622053 -1.499780 0.098119 -11.15764 -272.1797
219.7809 -241.8264 % H2O
        34.25667 55.18445 -35.15443 9.087440 -0.422157 -149.9098
257.0604 -136.1064 % H2O2
        20.78603 4.850638e-10 -1.582916e-10 1.525102e-11 3.196347e-11 211.8020
139.8711 217.9994 % H
        26.00960 34.85810 -16.30060 3.110441 -0.018611 -7.140991
250.7660 2.092001 % HO2
        52.02427 18.48801 -3.765128 0.248541 -12.45799 -85.53895
223.8022 -45.89806 % NH3
        60.30274 1.034566 -0.192997 0.012540 -6.860254 48.61390
272.5002 82.04824 % N2O
        35.99169 0.957170 -0.148032 0.009974 -3.004088 73.10787
246.1619 90.29114 % NO
        56.82541 0.738053 -0.144721 0.009777 -5.459911 2.846456
290.5056 33.09502 % NO2
        28.74701 4.714489 -0.814725 0.054748 -2.747829 26.41439
214.1166 38.98706]; % OH

```

```

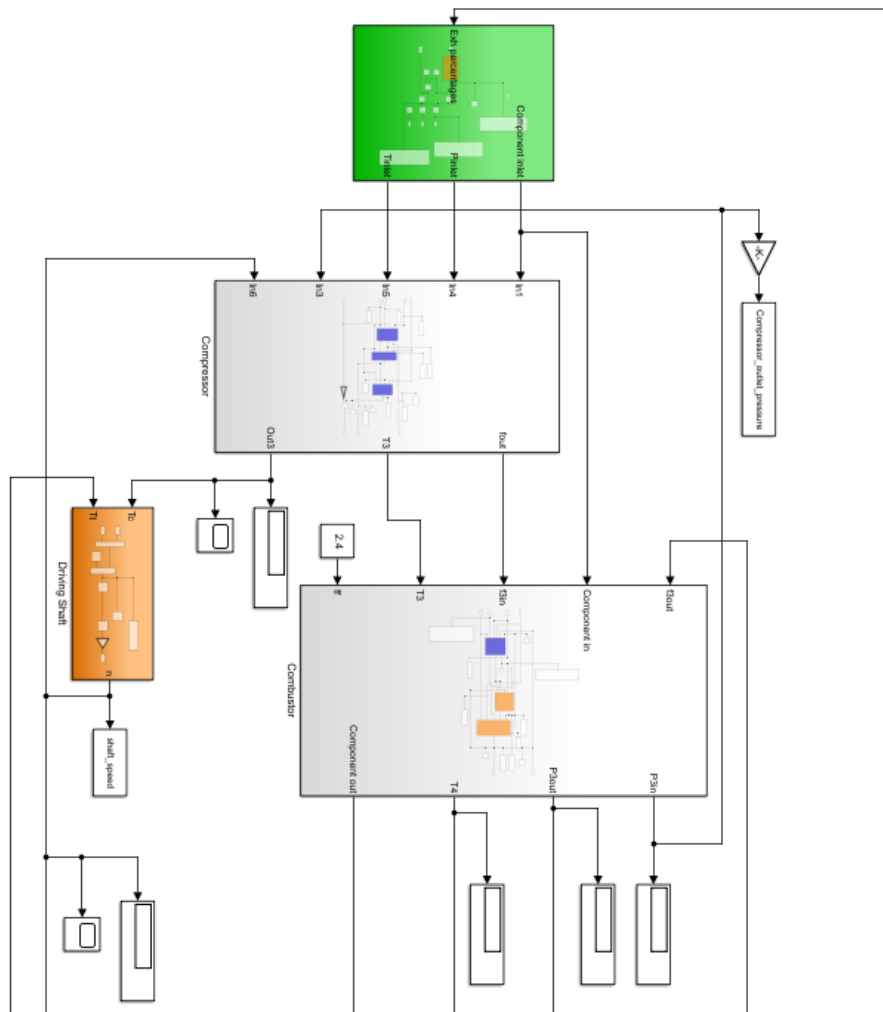
else
    WB = [35.51872 1.128728 -0.196103 0.014662 -4.553760 -18.97091
224.9810 0.0 % N2
        20.91111 10.72071 -2.020498 0.146449 9.245722 5.337651
237.6185 0.0 % O2
        20.78600 2.825911e-7 -1.464191e-7 1.092131e-8 -3.661371e-8 -6.197350
179.9990 0.0 % Ar
        18.563083 12.257357 -2.859786 0.268238 1.977990 -1.147438
156.288133 0.0 % H2
        41.96426 8.622053 -1.499780 0.098119 -11.15764 -272.1797
219.7809 -241.8264 % H2O
        34.25667 55.18445 -35.15443 9.087440 -0.422157 -149.9098
257.0604 -136.1064 % H2O2
        20.78603 4.850638e-10 -1.582916e-10 1.525102e-11 3.196347e-11 211.8020
139.8711 217.9994 % H
        45.87510 8.814350 -1.636031 0.098053 -10.17380 -26.90210
266.5260 2.092001 % HO2
        52.02427 18.48801 -3.765128 0.248541 -12.45799 -85.53895
223.8022 -45.89806 % NH3
        60.30274 1.034566 -0.192997 0.012540 -6.860254 48.61390
272.5002 82.04824 % N2O
        35.99169 0.957170 -0.148032 0.009974 -3.004088 73.10787
246.1619 90.29114 % NO
        56.82541 0.738053 -0.144721 0.009777 -5.459911 2.846456
290.5056 33.09502 % NO2
        28.74701 4.714489 -0.814725 0.054748 -2.747829 26.41439
214.1166 38.98706]; % OH
end

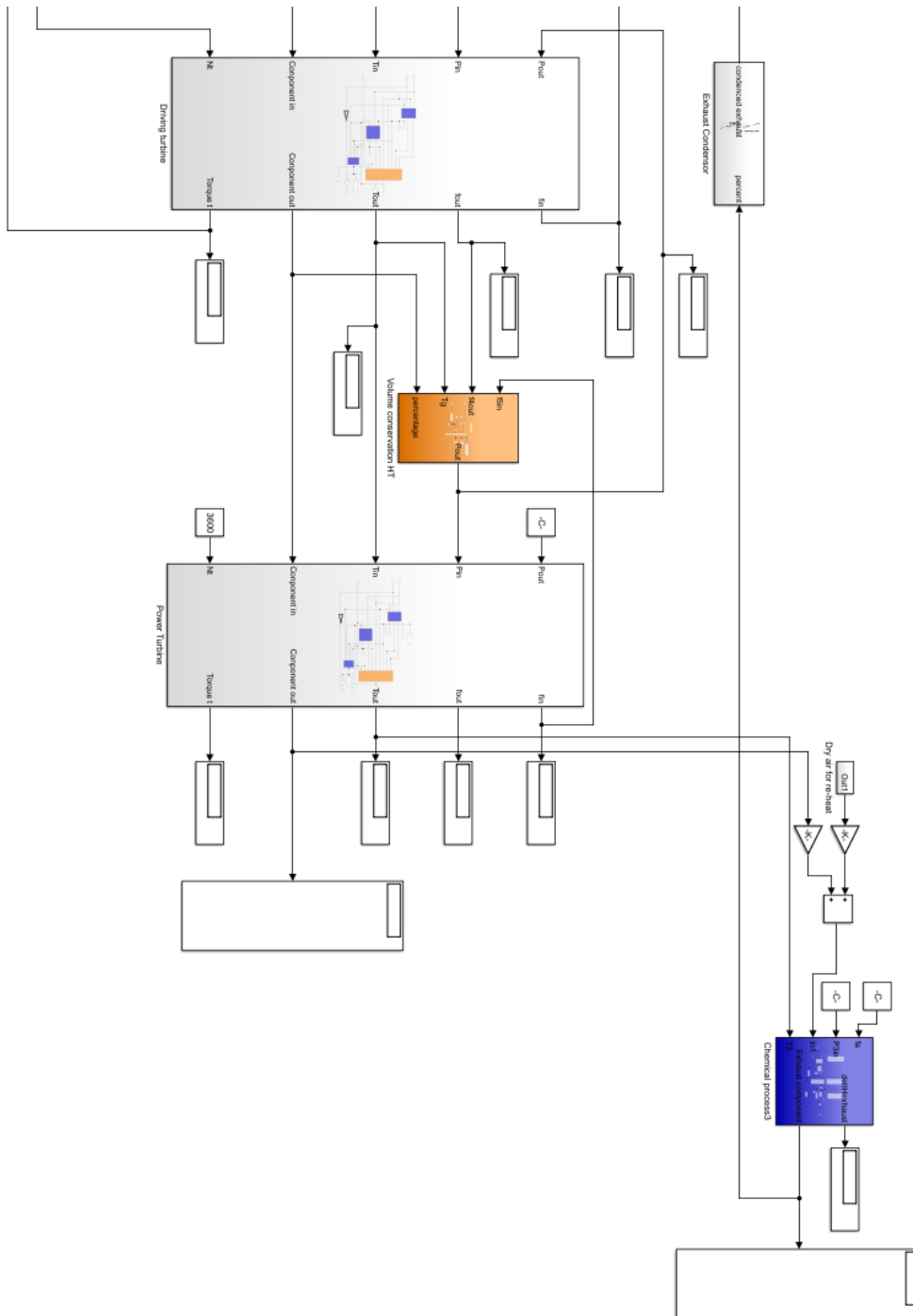
Ho = WB*T_Ho;
% (H - H_298.15) kJ/mol Hf_298 has been added with the NIST H factor being o
H = WB*T_H;
% (H - H_298.15) kJ/mol Hf_298 has been added with the NIST H factor being o
S = WB*T_S/1000;
% Absolute entropy kJ/mol/K
function G = func(nj)
%fmincon solver target function, Gibbs free
    Enj = sum(nj);
    S = WB*T_S/1000;
    % Absolute entropy kJ/mol/K
    Gjo = H - T.*S;
    % Gibbs free energy of each component at T
    G = sum(nj.*(Gjo'/R/T + log(nj/Enj*P/Po)));
    %Summarize the free energy
end
% species = {'N2' 'O2' 'Ar' 'H2' 'H2O' 'H2O2' 'H' 'HO2' 'NH3' 'N2O' 'NO' 'NO2' 'OH'};
Aeq = [ 0 2 0 0 1 2 0 2 0 1 1 2 1 % O balance
        0 0 0 2 2 2 1 1 3 0 0 0 1 % H balance
        2 0 0 0 0 0 0 0 1 2 1 1 0 % N balance
        0 0 1 0 0 0 0 0 0 0 0 0 0 ];% Ar balance
LB = [0 0 0 0 0 0 0 0 0 0 0 0 0];
% LB for fmincon solver
options = optimset('Algorithm','sqp');
% Option for fmincon
x1 = fmincon(@func,xo,[],[],Aeq,beq,LB,[],[],options);
% fmincon solver delivering chemical outputs
Htoto = sum(xo.*(Ho'));
% Calculate input enthalpy as ref.
Htot = sum(x1.*H');
% Calculate generated enthalpy using fmincon outputs
Hbalance = Htot - Htoto;
% Enthalpy balancing
end
end

```


B | GENERAL VIEW OF THE SIMULINK MODEL

The following plots shows the general layout of the Simulink model of this project. The green block represents the EGR system. Chemical solvers and static principles of the gas turbine system are covered in blue formats. The dynamic conservation functions are marked with orange. Notice that the model has been divided into two plots at the outlet of the combustor, and the **HRSG!** (**HRSG!**) re-heater is connected to the outlet of the power turbine sub-system.







STATIC RESULTS

Fuel injection (kg/s)	4.0	3.6	3.2	2.8	2.4	2.0	1.6
Fuel injection ratio (%)	100	90	80	70	60	50	40
Compressor air flow (kg/s)	40.0	36.0	32.0	28.0	24.0	20.0	16.0
Compressor PR	20.00	17.42	15.47	13.22	10.89	8.95	6.71
Compressor efficiency (%)	82.00	80.61	78.50	74.97	69.96	64.23	55.80
Compressor outlet temperature (K)	82.00	80.61	78.50	74.97	69.96	64.23	55.80
Shaft speed (rpm)	9600	8985	8728	8467	8208	7933	7614
Shaft speed ratio (%)	100.00	93.59	90.92	88.20	85.50	82.64	79.31
TIT (K)	1542	1519	1505	1490	1475	1464	1448
High pressure turbine PR	3.514	3.390	3.368	3.410	3.535	3.751	4.175
High pressure turbine efficiency (%)	87.00	85.61	83.61	80.42	76.09	71.24	64.26
High pressure turbine outlet temperature (K)	1207	1202	1200	1196	1192	1191	1187
Power turbine PR	5.692	5.138	4.594	3.877	3.081	2.386	1.607
Power turbine efficiency (%)	89.00	88.69	85.77	84.95	79.32	70.75	52.86
Exhaust temperature (K)	842.7	857.6	879.3	915.3	969.2	1033	1120
Gas turbine power output (MW)	25.80	21.98	18.24	14.02	9.58	5.70	1.95
Power output ratio (%)	100.00	85.19	70.70	54.34	37.15	22.09	7.57
Gas turbine system efficiency (%)	34.68	32.83	30.65	26.92	21.47	15.32	6.56
Re-heat temperature (K)	1267	1281	1303	1339	1394	1461	1559
HRRSG heat-flow (MJ/s)	60.08	54.99	50.05	45.53	41.31	36.77	32.11
Molar H ₂ in exhaust (%)	6.617	6.617	6.617	6.618	6.618	6.618	6.618
NOx emission (ppm)	9.161	10.56	12.63	18.18	25.27	35.30	39.25
NOx emission (g/kWh)	0.065	0.079	0.102	0.167	0.291	0.569	1.477
NOx emission (g/kgf)	1.169e-04	1.347e-04	1.612e-04	2.320e-04	3.224e-04	4.504e-04	5.008e-04

COLOPHON

This document was typeset using \LaTeX . The document layout was generated using the `arsclassica` package by Lorenzo Pantieri, which is an adaption of the original `classithesis` package from André Miede.

